

Modeling of a millisecond pulsed glow discharge: Investigation of the afterpeak

Annemie Bogaerts,^{*a} Renaat Gijbels^a and Glen P. Jackson^b

^aDepartment of Chemistry, University of Antwerp, Universiteitsplein 1, B-2610 Wilrijk-Antwerp, Belgium. E-mail: annemie.bogaerts@ua.ac.be

^bChemical Sciences Division, Oak Ridge National Laboratory, P.O. Box 2008, Oak Ridge, TN 37831-6375, USA

Received 20th December 2002, Accepted 10th February 2003

First published as an Advance Article on the web 20th February 2003

We have developed a comprehensive modeling network for a millisecond pulsed glow discharge in argon (Ar) with copper (Cu) cathode, to describe the behavior of the various plasma species. Typical results of the model are shown, such as the potential distribution during and after the pulse, the densities of Ar⁺ ions, Ar atoms in the metastable and various other excited levels, Cu atoms and Cu⁺ ions, in ground state and excited levels, as well as optical emission intensities as a function of time during and after the pulse. Special attention is paid to the mechanisms giving rise to the so-called “afterpeak”, *i.e.*, the peak in Ar and Cu excited level populations and optical emission intensities, which is experimentally observed in the afterglow of pulsed discharges. This afterpeak is attributed to electron-ion recombination to the highest excited levels, followed by radiative decay to lower levels. It is expected that the electron temperature decreases drastically upon pulse termination, resulting in a significant rise in electron density, making electron-ion recombination more plausible. Because we were not yet able to model these mechanisms, we worked in reversed order, to find out which recombination mechanisms account for the experimentally observed afterpeaks. Collisional-radiative recombination (*i.e.*, three-body recombination with an electron as the third body) is the most plausible candidate, both for Ar and Cu, but it requires a rise in electron density in the afterglow, estimated to be about two orders of magnitude relative to the steady state, or voltage-on period. Therefore, as an alternative, we think that dissociative recombination of Ar₂⁺ ions in high vibrational levels cannot yet completely be ruled out.

1. Introduction

Pulsed glow discharges are gaining increasing interest in the analytical community, because they have some inherent advantages compared to direct current (dc) glow discharges.^{1–3} Indeed, because the voltage and current are only applied during short periods of time, much higher peak voltages and currents can be obtained for the same average electrical power, giving rise to higher signal intensities, and hence better analytical sensitivities.^{4–7} Moreover, background signals can be reduced when time-resolved detection is applied, because analyte and background species appear to be formed at different times in or after the pulse.^{8–14} Some other characteristics are the low overall sputter rates (in combination with high transient sputter rates and hence high signal intensities) opening possibilities in the field of thin film analysis^{15,16} (in fact, a wide dynamic range of layers, from several nm to tens of μm thick, can be analyzed¹⁷), as well as the ability to obtain structural, molecular and elemental information of samples.^{18,19} Indeed, depending on the extent of interaction with the plasma, the samples may undergo soft chemical ionization yielding molecular ions or they may be completely atomized and ionized, yielding elemental information. Pulsed glow discharges have been coupled to atomic emission, absorption and fluorescence spectrometry, as well as to mass spectrometry.^{1–30} Both millisecond (ms) and microsecond (μs) pulsed discharges have been (and still are) the subject of investigation, not only to improve the analytical characteristics, but also from fundamental point of view, to obtain a better insight in the ionization and excitation mechanisms.^{4,25–30}

In the past decade, we have developed a number of models to describe the behavior of the various plasma species in analytical glow discharges (*e.g.*, ref. 31). This “modeling network” has

been applied to direct current (dc), radio-frequency (rf) and μs -pulsed operation modes. Whereas dc and rf discharges are rather well-described with our models (*e.g.*, refs. 31–33), this is not yet the case for the μs -pulsed glow discharge. Indeed, our model calculations^{34,35} were compared with experimental data from Harrison *et al.* The experimental data showed a pronounced peak in the electrical current, in the beginning of the pulse, but in order to predict this in our model, we had to assume a considerable variation of the gas temperature as a function of time.³⁴ In connection with the discussion about this characteristic behavior of the electrical current, Harrison and coworkers repeated their experiments, and found out that the initial current peak had to be attributed to the measuring circuit (capacitive effects) and not to the real plasma current.³⁶ Hence, our assumptions made in the μs -pulsed model about the time-behavior of the gas temperature,³⁴ are not valid anymore. Another point of discussion, which emerged from our modeling calculations, is the presence of the peak in excited level populations, optical emission intensities and analyte ion signals in the afterglow, when the pulse is terminated. This experimentally observed “afterpeak” is attributed in the literature (*e.g.*, refs. 25–30) to electron-ion recombination. However, when we applied our modeling network to the pulsed glow discharge, using the calculated electron and ion densities and the rate constants for electron-ion recombination (adopted from the literature), electron-ion recombination appeared not to be important enough to give rise to an afterpeak.^{34,35} The same conclusion was independently also drawn by Jackson.³⁰ This suggests that maybe some physical processes are still overlooked in the model.

Therefore, in the present work, we want to investigate in more detail which electron-ion recombination mechanisms might be responsible for the experimentally observed afterpeak. For

this purpose, we have applied our modeling network to a millisecond pulsed glow discharge, which has recently been the subject of some very interesting diagnostic investigations by King and coworkers.^{28–30} Indeed, this group measured the two-dimensional spatial distributions of the copper (Cu) atom and ion ground state and excited levels, and of the metastable argon (Ar) atoms as a function of time, by atomic absorption, emission and/or laser-induced fluorescence spectrometry, and they focussed especially on the afterpeak behavior. In Section 2, we will briefly describe our modeling work, and we will point out the characteristic aspects of modeling the ms-pulsed glow discharge. Section 3 contains the results, as well as a discussion on the mechanisms responsible for the afterpeak behavior. Finally, the conclusion will be given in Section 4.

2. Description of the modeling network

It is important to appreciate that low pressure gas discharges that are supported by an electric field are seldom close to equilibrium conditions. For this reason, the Boltzmann, Planck and other equilibrium equations that are usually used to predict the distribution of states are no longer accurate. The disequilibrium makes it necessary to calculate the population and depopulation rate of every state in the plasma in order to predict its population density, which is where the modeling network arises.

The modeling network consists of several sub-models to describe the behavior of the various plasma species. We consider a glow discharge in Ar, with Cu as the cathode material. The species assumed to be present in the plasma are the Ar gas atoms, the electrons, the Ar⁺ ions, the fast Ar atoms, the Ar atoms in various excited levels, the sputtered Cu atoms and the corresponding Cu⁺ ions, both in the ground state and in various excited levels. The Ar atoms are assumed to be uniformly distributed in the plasma, and in thermal equilibrium with the gas temperature; and no specific model is applied to describe their behavior. The other species are simulated by a number of Monte Carlo, fluid and collisional-radiative models. The choice of a particle model depends on the type of species and their energy. Briefly speaking, Monte Carlo models, which are very accurate but computationally rather time-consuming, are applied to the fast (energetic) plasma species that are not in equilibrium with the electric field. The species described by this model gain more energy from the electric field than they lose by collisions with low energy particles. Faster than the Monte Carlo model is the more approximate fluid model that is based on the assumption that the particles are in equilibrium with the electric field. It applies to the slow plasma species, for which this assumption is reasonably valid. Finally, a collisional-radiative model is a kind of fluid model, which is specifically used for excited species (see below). In the following, these models will be briefly described.

2.1. Monte Carlo model for the fast electrons

The electrons are split up in two groups depending on their energy. The fast (or energetic) electrons, *i.e.*, with total (= sum of potential and kinetic) energy above the threshold for inelastic collisions, are simulated with a Monte Carlo model, whereas the slow electrons (*i.e.*, with energy below this threshold) are described in a fluid code. The Monte Carlo model follows a large number of individual “super-electrons” (which represent a number of real electrons), one after the other, as a function of time during and after the pulse. Their trajectory under the influence of the electric field is calculated by Newton’s laws, and their collisions (*i.e.*, occurrence of a collision, kind of collision, new energy and direction after collision) are treated with random numbers. The collisions taken into account are elastic collisions with Ar gas atoms, as well as ionization and excitation of the Ar atoms in the ground

state and in the metastable levels, and ionization of the sputtered Cu atoms. Details about the Monte Carlo procedure (cross sections, scattering, *etc.*) can be found, *e.g.*, in ref. 37.

2.2. Fluid model for the slow electrons and Ar⁺ ions

When the fast electrons have lost so much energy due to collisions that their energy drops below the threshold for inelastic collisions (*i.e.*, ionization and excitation), they are transferred to the slow electron group which is described with a fluid model.

Besides the slow electrons, the fluid model simultaneously treats the Ar⁺ ions. The fluid model consists of the continuity (balance) equations with source terms (production rates) adopted from the above Monte Carlo model and transport equations, based on diffusion and migration in the electric field, of the slow electrons and Ar⁺ ions. These equations are coupled to each other, as well as to Poisson’s equation for a self-consistent calculation of the electric field distribution. Because these differential equations are strongly coupled and severely non-linear, solving this system of coupled equations is a difficult numerical problem. For more details about this model (equations, input data, solution procedure,...) we refer to ref. 38.

2.3. Monte Carlo model for the fast Ar⁺ ions and fast Ar atoms in the cathode dark space (CDS)

The region near the cathode that is characterized by a strong electric field is commonly known as the CDS. Because the Ar⁺ ions are not in equilibrium with the electric field in the CDS they are described in this region not only with a fluid model, but also with a Monte Carlo approach. This model yields, among others, the flux energy distribution of the Ar⁺ ions bombarding the cathode, which is important in calculating the sputtering rate (see below).

Because the fast Ar atoms are created *via* elastic collisions with fast Ar⁺ ions in the CDS the Ar gas atoms are also simulated with the Monte Carlo model. Indeed, it has been demonstrated³¹ that fast Ar atoms play a dominant role in cathode sputtering; hence, we need to compute the flux energy distribution of fast Ar atoms in a Monte Carlo model in order to calculate the amount of sputtering. More information about these Monte Carlo models (collision processes taken into account, corresponding cross sections, scattering theories, *etc.*) can be found in refs. 37 and 39.

2.4. Collisional-radiative model for the Ar atoms in excited levels

Because we want to investigate the behavior of the excited level populations and optical emission intensities during and especially after the pulse, the so-called “afterpeak”, a detailed model for the description of the excited levels is necessary. In a collisional-radiative model, the level populations of the excited levels are calculated with a set of balance equations (one for each level), with different production and loss terms. We consider 64 Ar atom excited levels; some of them are individual levels (*e.g.*, the four 4s levels), but most of them are “effective” levels, consisting of several individual levels with similar excitation energy and quantum numbers.

The production and loss processes taken into account are all collisional or radiative processes; hence the name of this model. They include electron, ion and atom excitation, de-excitation and ionization from all levels, electron-ion recombination to the highest excited levels, radiative decay between all levels (allowed transitions), and Hornbeck–Molnar associative ionization (*i.e.*, Ar^{**} + Ar⁰ → Ar₂⁺ + e⁻) for the Ar levels with excitation energy above 14.7 eV. Note that for most excited levels, radiative decay is the dominant loss mechanism.

Moreover, some additional processes are incorporated for

the 4s levels. Two of them, *i.e.*, the 4s 3P_2 and 4s 3P_0 levels (lying at 11.55 and 11.72 eV above the ground state, respectively) are metastable, *i.e.*, they cannot decay to the ground state by emission of radiation (forbidden transitions). The two other 4s levels, *i.e.*, the 4s 3P_1 and 4s 1P_1 levels (at 11.62 and 11.83 eV above the ground state, respectively) can decay to the ground state by emission of radiation, but the emitted photons will very easily be re-absorbed by the ground state atoms, so that only a small fraction of the emitted radiation can escape. The so-called “escape factor” is in the order of 10^{-3} ; hence about 99.9% re-absorption.⁴⁰ Hence, all four 4s levels are characterized by a rather high population density. Because radiative decay is not possible or not efficient for these 4s levels, some additional loss processes are incorporated. These metastable atom loss processes include Penning ionization of the sputtered atoms, two-body and three-body collisions with Ar gas atoms, collisions between two atoms in 4s levels leading to either ionization of one of the atoms or to associative ionization: Ar_2^+ , and transport by diffusion. More information about this model can be found in ref. 40.

2.5. Sputtering at the Cu cathode

The flux of sputtered Cu atoms from the cathode is calculated from the flux energy distributions of the energetic plasma species bombarding the cathode, multiplied by the sputter yield at each bombarding energy. The sputter yield is calculated with an empirical formula.⁴¹ The plasma species playing a role in the cathode sputtering, are the Ar^+ ions and the fast Ar atoms (see above), as well as the Cu^+ ions, created in the plasma from the sputtered Cu atoms (leading to so-called self-sputtering, see below). The flux energy distributions of these species at the cathode are calculated with Monte Carlo algorithms (see above and below).

2.6. Monte Carlo model for the thermalization of the sputtered Cu atoms

When the Cu atoms are sputtered from the cathode, they have typical energies in the order of a few eV, which they lose very rapidly by collisions with the Ar gas atoms, until they are thermalized. This thermalization process as a result of collisions is simulated with a Monte Carlo approach. The output of this model is the so-called “thermalization profile”, *i.e.*, the number of sputtered Cu atoms as a function of position from the cathode, which is used as input in the next model. Indeed, once the Cu atoms are thermalized, their further transport is diffusion-dominated, and since the thermalization process takes place at a much shorter time-scale than diffusion, thermalization can be assumed to be complete before significant diffusion occurs. Hence, the thermalization profile is used as “initial spatial distribution” of the sputtered Cu atoms. More details about this Monte Carlo model for thermalization can be found in ref. 42.

2.7. Collisional-radiative model for the Cu atoms and Cu^+ ions in the ground state and in various excited levels

The sputtered Cu atoms will be subject to ionization and excitation in the plasma. The behavior of the Cu atoms and Cu^+ ions in the ground state and excited levels is described with a collisional-radiative model, in analogy to the collisional-radiative model for the Ar excited atoms. Eight Cu atom levels and seven Cu^+ ion levels are considered, as well as the Cu^{2+} ions. Most of these levels are again “effective” levels, *i.e.*, a group of individual levels with similar excitation energy and quantum numbers.

For each of these levels, a balance equation is again constructed, with different production and loss terms. The production and loss processes taken into account, include electron and atom impact ionization, excitation and de-excitation

between all levels, electron-ion recombination to the highest excited levels, radiative decay between all levels, as well as Penning ionization of Cu atoms by Ar metastable atoms and asymmetric charge transfer between Cu atoms and Ar^+ ions. Furthermore, a transport equation is solved for the Cu atoms (based on diffusion) and for the Cu^+ and Cu^{2+} ions (based on diffusion and on migration in the electric field). For more information about this model (*e.g.*, levels considered, equations, input data for these processes, solution algorithm,...) we refer to ref. 43.

2.8. Monte Carlo model for the Cu^+ ions in the CDS

Finally, in the CDS, the trajectory and collisions of Cu^+ ions are also followed with a Monte Carlo algorithm. Among other details, this model also predicts the flux energy distribution at the cathode, needed to compute the flux of sputtered Cu atoms.

2.9. Coupling of the models

All these models are coupled to each other due to the interaction processes between the different species, and they are solved iteratively until final convergence is reached. This typically takes a few days on today’s fast computers. The Monte Carlo models are developed fully in three dimensions, whereas the fluid and collisional-radiative models are two-dimensional. Indeed, due to the cylindrical symmetry of the glow discharge source under study (see later), the three dimensions could be reduced to two dimensions (*i.e.*, axial and radial direction).

2.10. Application of the modeling network to a millisecond-pulsed glow discharge

The model is applied to the millisecond (ms)-pulsed glow discharge, investigated experimentally by King and co-workers.^{28–30} The glow discharge source studied experimentally was a six-way cross cell, with a cathode of 4 mm diameter. Data were collected for 1.8 cm in the axial direction (*i.e.*, perpendicular to the cathode surface) and 2 cm in the direction parallel to the cathode surface. Because the measured two-dimensional spatial distributions appeared to be symmetric with respect to the cell axis,^{28–30} we have approximated this cell geometry by a cylinder, with length of 1.8 cm and diameter of 2 cm. The cathode diameter is taken as 4 mm (see above).

A pulse of 5 ms is applied, with a frequency of 50 Hz. Hence, the total period is 20 ms, and the intermediate time between two pulses is 15 ms (25% duty cycle). The gas pressure is 0.8 Torr, and the gas temperature (unknown from experiment) is assumed to be 540 K. Peak voltage and current are 860 V and 1.8 mA.^{28–30} Fig. 1 shows the voltage (a), current (b) and electric power (c) as a function of time during and after the pulse. The voltage as a function of time is adopted from experiment,²⁹ and is used as input in the model. The electric current and power are calculated in the model, and appear to follow the time-behavior of the voltage. A gas temperature of 540 K was assumed in the model, because it yields a peak electric current of 1.8 mA, in agreement with the experimental value. Finally, the electric power is simply the product of voltage and current, as is clear from Fig. 1(c).

The discharge characteristics have to be modeled as a function of time (during and after the pulse). We have checked that the intermediate time between two pulses is sufficiently long, so that the plasma is extinguished before the next pulse starts. Hence, every pulse behaves identically, and we have to run the models only during one pulse followed by its afterglow. However, even this time-scale is very long compared to the characteristic time-step in the Monte Carlo models (*i.e.*, typically 3×10^{-12} s to describe the electron behavior; somewhat longer for the heavy particles). Hence, the Monte Carlo models would have to be run for an extremely large number of

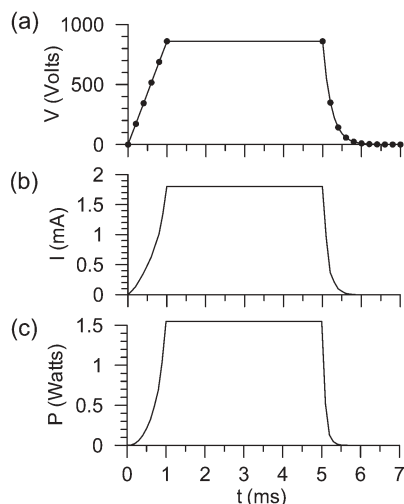


Fig. 1 Applied voltage (a), and calculated electric current (b) and power (c), as a function of time during and after the pulse, for a pulse length of 5 ms, a pulse repetition frequency of 50 Hz, a pressure of 0.8 Torr, a gas temperature of 540 K, and a peak voltage and current of 860 V and 1.8 mA. The dots in Fig. 1a represent the moments in time at which the Monte Carlo models are followed (see text).

time-steps, leading to an excessively long computation time. To solve this problem, we have followed the plasma species in the Monte Carlo models only at a fixed number of moments in time, until steady-state was reached (which occurs actually rather quickly, compared to the ms-timescale). In practice, five points were taken during the rise-time of the pulse voltage, of which the last point corresponds to the constant period of the pulse (and is assumed to be representative for the entire constant period), and ten points during the afterglow period (see Fig. 1(a)). In the fluid and collisional-radiative models, however, the build-up and decay in the densities and level populations really have been followed as a function of time, and not only at the discrete times. Hence, the input from the Monte Carlo models (*e.g.*, production and loss rates) at the discrete times, have been interpolated to the intermediate times.

3. Results and discussion

3.1. Electric potential distribution

The potential applied between the two electrodes was plotted as a function of time in Fig. 1(a). It is not uniformly distributed over the plasma, but it drops rapidly in the cathode dark space (CDS) from a negative value at the cathode towards zero at a few mm from the cathode. In the negative glow (NG), the potential is slightly positive and nearly constant, giving rise to a weak electric field. The calculated potential distribution in the axial direction (and at the cell axis) is presented in Fig. 2, at different times.

During the pulse rise-time (Fig. 2(a)), the potential at the cathode ($z = 0$ cm) becomes gradually more negative as a function of time, as was also shown in Fig. 1(a). The potential in the NG appears to reach the same value (about 30 V) from the beginning of the pulse rise-time, *i.e.*, as soon as the CDS and NG start to develop, independent of the value of the cathode potential. When the pulse is terminated (Fig. 2(b)), the cathode potential becomes gradually less negative as a function of time, as was also seen in Fig. 1(a). Furthermore, the value in the NG decreases as well. Hence, this shows that the clear subdivision in CDS and NG disappears, which illustrates the extinguishing character of the plasma. At 6 ms (*i.e.*, 1 ms after pulse termination), the potential drop, and hence the electric field, have become very small, as follows from Fig. 2(b).

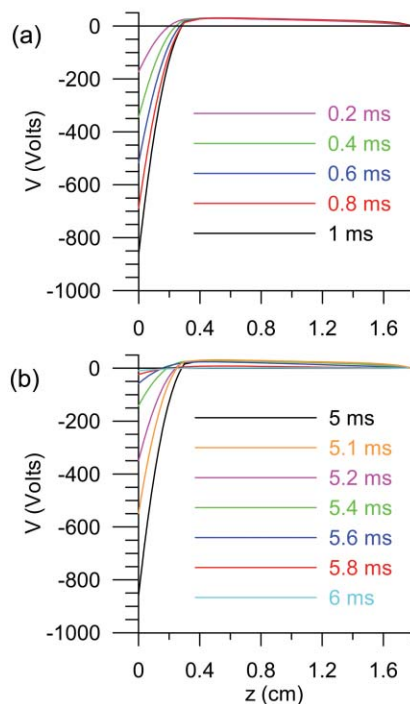


Fig. 2 Calculated one-dimensional electric potential distributions, at different times, (a) during the pulse rise-time, and (b) in the afterglow, for the same conditions as in Fig. 1. The cathode is located at $z = 0$ cm, whereas $z = 1.8$ cm represents the back end of the cell, at anode potential (grounded).

3.2. Electrons and Ar⁺ ions

The calculated one-dimensional Ar⁺ ion density profiles (*i.e.*, in the axial direction, and averaged in the radial direction over the region of the cathode diameter) are presented in Fig. 3, at the same times and for the same conditions as in Fig. 2. The qualitative behavior is the same for all profiles, with a low and

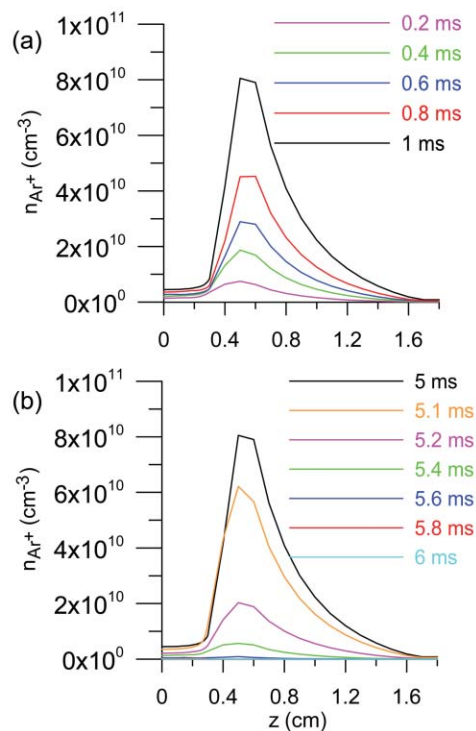


Fig. 3 Calculated one-dimensional density profiles of the Ar⁺ ions, at different times, (a) during the pulse rise-time, and (b) in the afterglow, for the same conditions as in Fig. 1.

nearly constant value in the CDS, and a maximum in the NG. Note that the electron densities are characterized by a similar profile, except that they are zero in the CDS.

As expected, the Ar^+ and electron densities increase as a function of time during the pulse rise-time (Fig. 3(a)) because the increasing electric field results in more ionizing collisions, hence the creation of more electrons and Ar^+ ions. After pulse termination, the calculated Ar^+ ion and electron densities appear to drop as a function of time (Fig. 3(b)), for the same reason, *i.e.*, the removal of the electric field results in a removal of the ionization collisions. However, it should be noted that the latter calculation result does probably not reflect reality, at least not for the behavior of the electron density in the afterglow.

Indeed, in reality it is expected that upon pulse termination the electron population will thermalize to the gas temperature.^{30,44} This is because there is no longer an electric field to accelerate and heat them any more and they will lose their energy *via* collisions. Consequently, the thermalized electrons will not be able to reach the cell walls very easily because their transport (by diffusion) becomes very slow; they will be more or less “trapped” in the bulk of the afterglow plasma. Hence, it is expected that their density rises considerably.⁴⁴

Unfortunately, this behavior cannot be simulated with our fluid model because the latter contains only the continuity and transport equations and no electron energy balance equation. In fact, even if such an energy balance equation would have been included (as was the case in our fluid model for the rf mode⁴⁵), the calculated electron energy would still be very approximate, and we would not be able to predict the thermalization behavior and the correct rise in electron density. For this purpose, a particle-in-cell/Monte Carlo (PiC/MC) approach would have to be applied,^{46,47} but the latter would take an extremely long calculation time, making it practically impossible to describe correctly the thermalization of these electrons with very high density.

Since the exact rise of the electron density in the afterglow cannot yet be simulated in our model, and since this quantity has also not yet been measured in the ms-pulsed glow discharge, we are not able to calculate in a reliable way the behavior of the other plasma species, and more specifically the level populations of the excited levels, and optical emission intensities. Indeed, it is generally accepted in the literature that the observed rise in excited level populations, and corresponding optical emission intensities, in the afterglow is attributed to ion-electron recombination. This was not only pointed out for analytical pulsed glow discharges (*e.g.*, refs. 25–30), but also in other types of afterglow (or recombining) plasmas, used to study the basic mechanisms of recombination (*e.g.*, refs. 48–50). The mechanism characteristic for these recombining plasmas, is called “capture-radiative-cascade” (CRC)^{50–52}: electron-ion recombination (or “electron-capture”) populates the highest excited levels, which subsequently decay radiatively to lower excited levels (“radiative cascade”). Hence, based on these considerations, the electron density should be known very accurately before we can make reliable predictions on the excited level populations.

Therefore, we will have to work in “reversed order”. King and coworkers have measured the Ar metastable densities and the optical emission intensities of various Ar and Cu lines (which correlate to the excited level populations) at different times during and after the pulse, in the ms-pulsed glow discharge under study.^{28–30} We have compared these experimental data with our calculation results, using different values for the recombination rate as input in the collisional-radiative models (*i.e.*, as production process for the excited levels). More specifically, the mechanism of CRC is simulated here: electron-ion recombination populates the highest excited levels, whereas radiative decay from these levels yields subsequent production of the lower levels. From the values of the recombination rate,

which give reasonable correlation between calculated and experimental data for the excited level populations and optical emission intensities, we hope to elucidate which recombination mechanisms result in a rise of the excited level populations in the afterglow, and what are the accompanying electron densities needed to give sufficient recombination.

Note that we do not tend to reach exact correlation with the experiment, which would never be possible in view of the complexity of the models required—especially the collisional-radiative model with the many excited levels and the large number of processes and considerable uncertainties in the input data. We only want to achieve a more or less realistic picture of the afterglow behavior, to obtain a better insight in the mechanisms responsible for the afterpeak. Therefore, a correlation with experimental data within an order of magnitude is considered sufficient for this purpose. In the following, we will first present our calculation results for the Ar atoms in excited levels, and for the Cu atoms and ions in the ground state and in excited levels. Subsequently, we will discuss which recombination mechanisms might be responsible for the afterpeak.

3.3. Ar atoms in excited levels

3.3.1. Ar atoms in the $(3p^5) 4s \ ^3P_2$ metastable level. Fig. 4 presents the calculated two-dimensional density profiles of the Ar atoms in the $(3p^5) 4s \ ^3P_2$ metastable level (Ar^*), at different times in the afterglow. Note that the cathode is situated at the bottom of the figure ($z = 0$ cm), around $r = 0$ cm, and with a diameter of 4 mm, whereas the other borders of the figure represent the cell walls, at anode potential.

At 5 ms (which corresponds to the end of the pulse, or the beginning of the afterglow) the calculated Ar metastable density reaches a maximum of $4.4 \times 10^{12} \text{ cm}^{-3}$ at about 1 mm from the cathode, and it drops significantly at distances further away from the cathode. This pronounced maximum near the cathode is due to fast Ar^+ ion, fast Ar atom and electron impact excitation.^{40,53}

At 5.1 ms, this maximum has slightly dropped to $3.2 \times 10^{12} \text{ cm}^{-3}$, and a second maximum (of $3.8 \times 10^{12} \text{ cm}^{-3}$) appears at 5–6 mm from the cathode. The latter is attributed in the model to electron-ion recombination to the highest excited Ar levels, followed by radiative decay to the Ar metastable level (CRC, see above). This mechanism is consistent with experimental results of Phelps and Molnar, who measured emission and absorption curves in a spark discharge in Ar, and observed that the maximum emission intensity occurs at the same time as the maximum rate of increase in the metastable density.⁵⁴ Beside these two maxima, the rest of the density profile remains nearly unchanged.

At 5.2 ms, the maximum near the cathode has disappeared, but the maximum at 5–6 mm is still of the same order, and the rest of the profile also remains the same. The same applies to 5.4 ms. At later times, the density drops slightly, but the position of the maximum and the rest of the density profile remain nearly unchanged. At 6 ms (*i.e.*, 1 ms after pulse termination) the maximum density is still about $2.7 \times 10^{12} \text{ cm}^{-3}$, and at 7 ms (*i.e.*, 2 ms after pulse termination) the maximum density is still in the order of 10^{12} cm^{-3} . Hence, the Ar^* metastable atoms are characterized by a rather long lifetime. The reason is that they cannot decay radiatively to lower levels, as is the case for the other Ar^* excited levels, and the other loss mechanisms take place on a longer timescale.⁵⁴

Comparing Fig. 4 with the measured two-dimensional density profiles of the $\text{Ar}^* 4s \ ^3P_2$ level by Jackson *et al.*,²⁹ tells us that our model sufficiently reflects the real afterglow behavior. Indeed, the disappearance of the first maximum at 1 mm from the cathode, and the appearance of the second maximum at 5–6 mm, are also found experimentally. The second maximum was measured to arise a bit later in time than predicted with our model. However, it is stated²⁹ that the

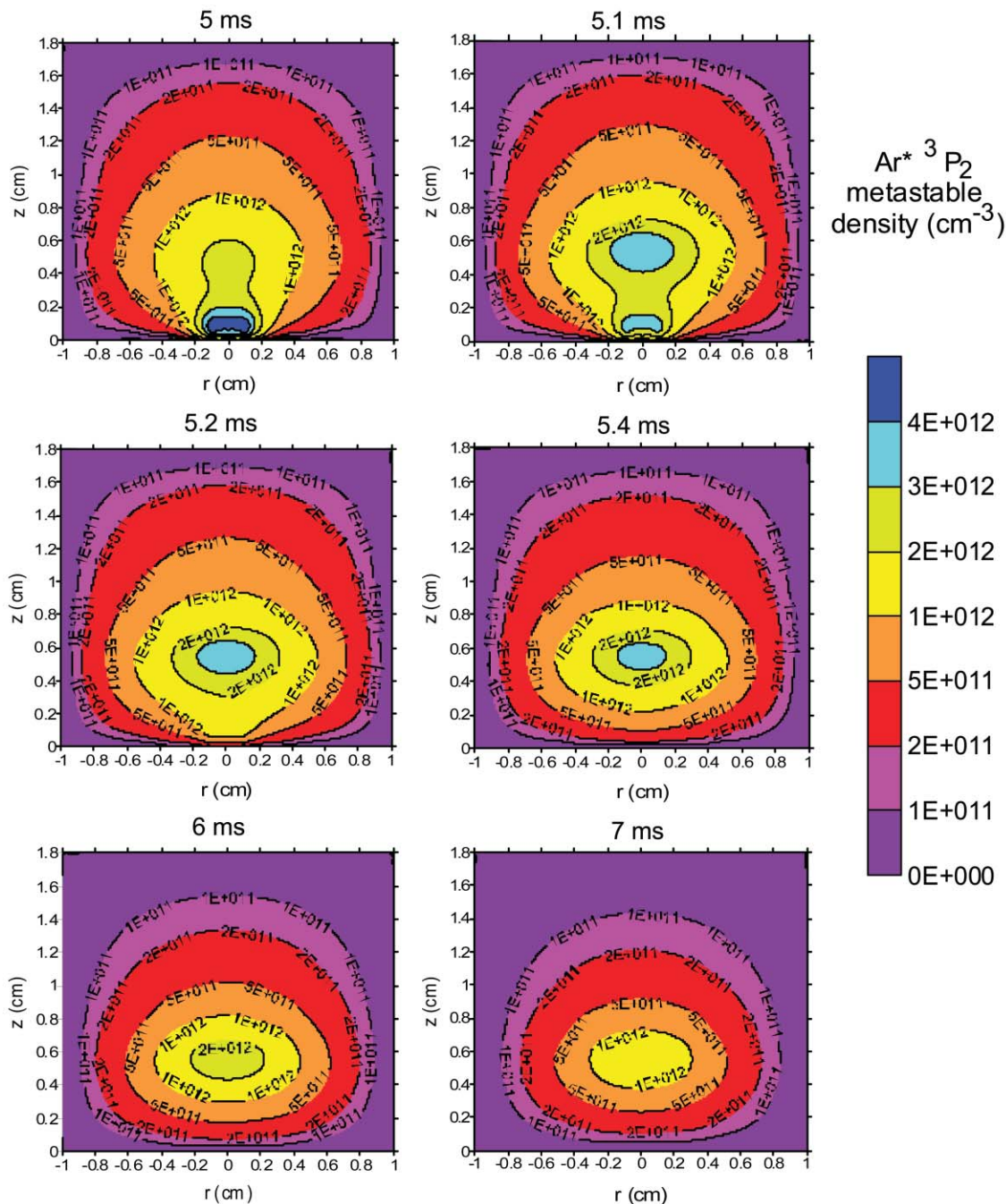


Fig. 4 Calculated two-dimensional density profiles of the $\text{Ar}(3p^5 4s^3 P_2)$ metastable atoms, at different times in the afterglow, for the same conditions as in Fig. 1. The cathode is located at the bottom (at $z = 0$ cm, around $r = 0$ cm), whereas the other borders of the figures represent the cell walls at anode potential.

temporal accuracy of the absorbance data was somewhat suspect, because of the RC time constant effect, and that the time domain should be used more as a relative index rather than absolute.²⁹ Moreover, as mentioned above, we do not tend to achieve exact correlation between our calculations and experiment, because this would be an impossible task, in view of the complexity of the model. For the purpose of investigation, we are satisfied when the general behavior is more or less in correspondence.

3.3.2. Ar atoms in metastable and other excited levels. In Fig. 5, the calculated one-dimensional density profiles (in the axial direction, *i.e.*, as a function of distance from the cathode, and averaged in the radial direction over the region of the cathode diameter) of various Ar^* excited levels are shown at different times in the afterglow. Note that $z = 0$ cm corresponds again to the cathode, whereas $z = 1.8$ cm corresponds to

the back end of the cell, at anode potential. The level populations at 5 ms, which represent the situation at the end of the pulse, or in the beginning of the afterglow, are plotted with a thicker black line.

Fig. 5(a) illustrates again that the $\text{Ar}^* 4s^3 P_2$ metastable level is characterized by a pronounced maximum near the cathode at 5 ms, which drops gradually as a function of time, and finally disappears at 5.2 ms. Moreover, the second maximum, at 5–6 mm from the cathode, attributed to electron-ion recombination followed by radiative decay, appears immediately after pulse termination, as is clear from Fig. 5(a).

The population density of the $\text{Ar}^* 4s^3 P_0$ metastable level is characterized by a similar behavior (see Fig. 5(b)), but the second maximum appears to be less pronounced, in comparison to the $\text{Ar}^* 4s^3 P_2$ metastable level. This suggests that electron-ion recombination, followed by radiative decay, would be less efficient in populating the $\text{Ar}^* 4s^3 P_0$ metastable

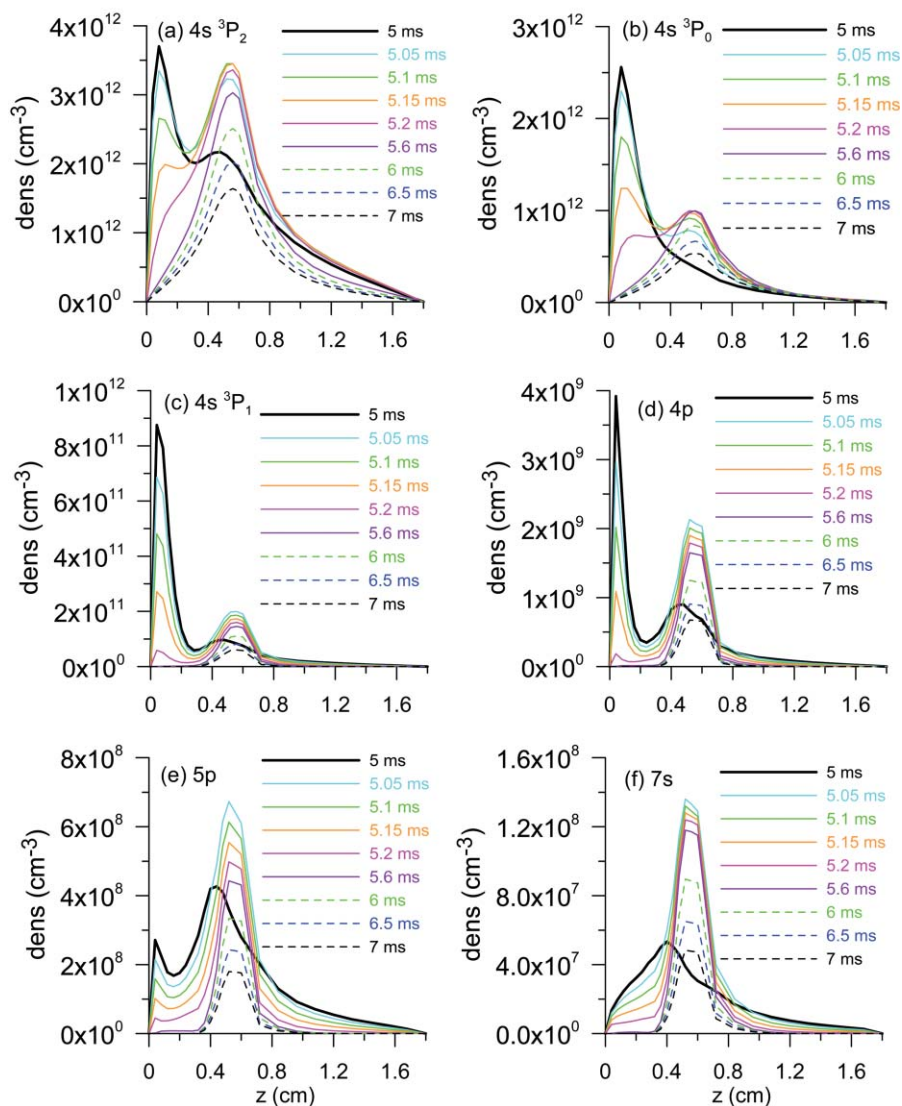


Fig. 5 Calculated one-dimensional density profiles of several Ar excited levels, at different times in the afterglow, for the same conditions as in Fig. 1. (a) Ar $4s\ ^3P_2$ metastable level (at 11.55 eV), (b) Ar $4s\ ^3P_0$ metastable level (at 11.72 eV), (c) Ar $4s\ ^3P_1$ level (at 11.62 eV), (d) an Ar $4p$ level (at 13.1 eV), (e) an Ar $5p$ level (at 14.5 eV), (f) an Ar $7s$ level (at 15.2 eV).

level than the Ar* $4s\ ^3P_2$ metastable level. This calculation result is in good correlation with experimental observations of Jackson *et al.*²⁹

Fig. 5(c) presents the density profiles of the Ar* $4s\ ^3P_1$ non-metastable level, at different times in the afterglow. At the end of the pulse, the calculated density of this level is characterized by a pronounced maximum near the cathode, mainly attributed to fast Ar⁺ ion and fast Ar atom impact excitation, which has disappeared 0.2–0.4 ms after pulse termination. At the same time, the second peak arises at 5–6 mm from the cathode, due to electron-ion recombination in the afterglow, followed by radiative decay. However, this second peak is quite low, which suggests that this level is again not populated so efficiently by radiative decay from the higher excited levels, compared to the Ar* $4s\ ^3P_2$ level. Moreover, it drops more quickly as a function of time, which reflects that the Ar* $4s\ ^3P_1$ non-metastable level has a shorter lifetime than the metastable levels.

The densities of the higher excited Ar* (non-metastable) levels are characterized by similar profiles, as is clear from Fig. 5(d)–(f). Note that the axial distributions of the excited level populations, during the pulse regime, are in good correlation with measured optical emission intensities of several Ar(I) lines originating from these levels.^{55,56} As the excitation energy increases ($4p \sim 13$ eV; $5p \sim 14.5$ eV; $7s \sim 15.2$ eV),⁴⁰ the maximum near the cathode at the end of the

pulse becomes less pronounced (or even disappears). Indeed, the higher levels cannot be populated by fast Ar⁺ ion and fast Ar atom impact excitation anymore, since these species have not enough energy. Moreover, the second maximum in the afterglow, at 5–6 mm from the cathode, becomes increasingly important for the higher excited levels, because they will be more efficiently populated by radiative decay from the highest levels produced by electron-ion recombination. Hence, the level populations of the higher excited levels will be characterized by a higher afterpeak/plateau ratio, compared to the lower excited levels.

3.3.3. Optical emission intensities of Ar(I) lines. The latter behavior also appears from Fig. 6, which shows the calculated optical emission intensities of some lines, characteristic for different upper levels, as a function of time during and after the pulse. The optical emission intensities were calculated by integration over the entire axial direction, to simulate end-on observation. The lines considered were taken the same as measured by Jackson *et al.*,³⁰ to allow direct comparison.

Comparing Fig. 6(a)–(d), it is clear that lines originating from higher excited levels are characterized by a higher afterpeak/plateau ratio, for the reason given above. This is in correlation with the experimental observations of Jackson *et al.*³⁰

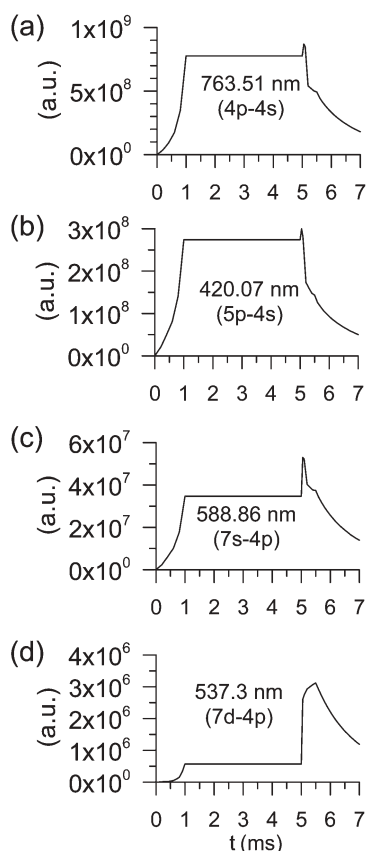


Fig. 6 Calculated optical emission intensities, integrated over the entire discharge length to simulate end-on observation, of some Ar(I) lines corresponding to different transitions, as a function of time, for the same conditions as in Fig. 1. (a) 763.51 nm (4p–4s transition), (b) 420.07 nm (5p–4s transition), (c) 588.86 nm (7s–4p transition), (d) 537.3 nm (7d–4p transition).

3.4. Sputtered Cu atoms and Cu⁺ ions

3.4.1. Sputtering. Fig. 7 shows the calculated flux of sputtered Cu atoms from the cathode, as a function of time during and after the applied voltage. The sputter flux clearly follows the same time-profile as the electric current, with a sharp rise at the start of the pulse, and a significant, fast drop after pulse termination. Indeed, the fluxes of the species responsible for the sputtering (*i.e.*, Ar⁺ ions, fast Ar atoms and Cu⁺ ions) all follow more or less the same time-behavior as the electric current. The Cu⁺ ions show a slight delay in time, because they first have to be formed and built up by sputtering and subsequent ionization, and moreover, their formation mechanism, due to Penning ionization by Ar metastable atoms, can also take place in the (early) afterglow (see later).

During the pulse rise-time, the relative contributions to

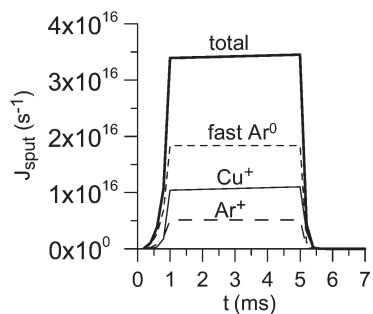


Fig. 7 Calculated flux of sputtered Cu atoms from the cathode as a function of time (thick solid line), as well as the contributions by fast Ar⁰ atoms (small dashed line), Cu⁺ ions (solid line) and Ar⁺ ions (wide dashed line), for the same conditions as in Fig. 1.

sputtering of the fast Ar atoms and Ar⁺ ions are in the order of 55–75% and 15–25%, respectively, decreasing as a function of time, because the relative contribution of Cu⁺ ions increases from 1 to 30%, as more and more Cu atoms and Cu⁺ ions are built up due to sputtering and subsequent ionization. During the plateau-regime, the relative contributions of fast Ar atoms, Ar⁺ ion and Cu⁺ ions are calculated to be about 55%, 15% and 30%, respectively. Note that the total sputter flux, as well as the contributions, were calculated to be nearly constant during this plateau-regime. However, we must admit that we did not look in detail at the plateau region of the pulse; we focused mainly on the afterglow. After pulse termination, the relative contributions of fast Ar atoms and Ar⁺ ions drop further as a function of time, whereas the Cu⁺ ions become increasingly important. At 5.8 ms, the sputtering is almost entirely attributed to the Cu⁺ ions (95%). However, it should be realized that at this time, the total amount of sputtering has already become very low.

3.4.2. Cu atoms in the ground state. In Fig. 8, the two-dimensional density profiles of the sputtered Cu atoms are plotted at different times in the afterglow. At the end of the pulse (5 ms), the Cu atom density reaches a pronounced maximum of $1.25 \times 10^{14} \text{ cm}^{-3}$ at about 1 mm from the cathode, and it drops towards low values at the cell walls. At 5.1 ms, the maximum has slightly decreased to about $8 \times 10^{13} \text{ cm}^{-3}$, but the shape of the density profile is unchanged. At later times, the maximum drops further, and shifts towards the middle of the discharge cell, as a result of diffusion. Note that the last two plots of Fig. 8 represents the data at 5.6 and 6 ms, in contrast to the density profiles of the Ar* metastable atoms (see above) and the Cu⁺ ions (see below), which show the data at 6 and 7 ms. According to the model, the Cu atoms have dropped to negligible values at 7 ms, so that it makes no sense to plot the density profile at this time.

The drop in Cu atom density is explained by the fact that there is no further production of Cu atoms (since the sputtering decreases significantly after pulse termination) and they can get lost by diffusion towards and subsequent deposition at the cell walls. A second maximum in the afterglow does not appear, which suggests that electron-ion recombination to the highest Cu* excited levels, followed by radiative decay is insignificant with respect to the quantity of ground state atoms already present. This is in good correlation with the experimental observations by Lewis *et al.*²⁸

3.4.3. Ionization of the Cu atoms. Fig. 9 shows the calculated ionization rate of the sputtered Cu atoms as a function of time during and after the pulse. The ionization rate also follows more or less the time-behavior of the electrical current. There is, however, a slight delay in the pulse rise-time, because the Cu atom density still has to build up. Moreover, a small increase in the ionization rate is predicted in the early afterglow, due to Penning ionization of the Cu atoms by the Ar* metastable atoms. The latter process was found to be the dominant ionization mechanism, with a relative contribution of about 97% during the plateau regime, increasing to 100% in the afterglow. Electron impact ionization and asymmetric charge transfer with Ar⁺ ions were calculated to contribute for about 2% and less than 1%, respectively. The reason for the predicted minor contribution of asymmetric charge transfer, is the much lower Ar⁺ ion density compared to the Ar* metastable density (*cf.* Figs. 3 and 4) and the bad overlap in density profiles of the Ar⁺ ions and sputtered Cu atoms (*cf.* Figs. 3 and 8). The ionization rate in Fig. 9 does not necessarily directly correlate to the ion signal observed in MS analyses because the loss rates are not taken into account. Also, this plot is an average over the entire discharge and not necessarily indicative of the ion signal expected at any individual sampling point.

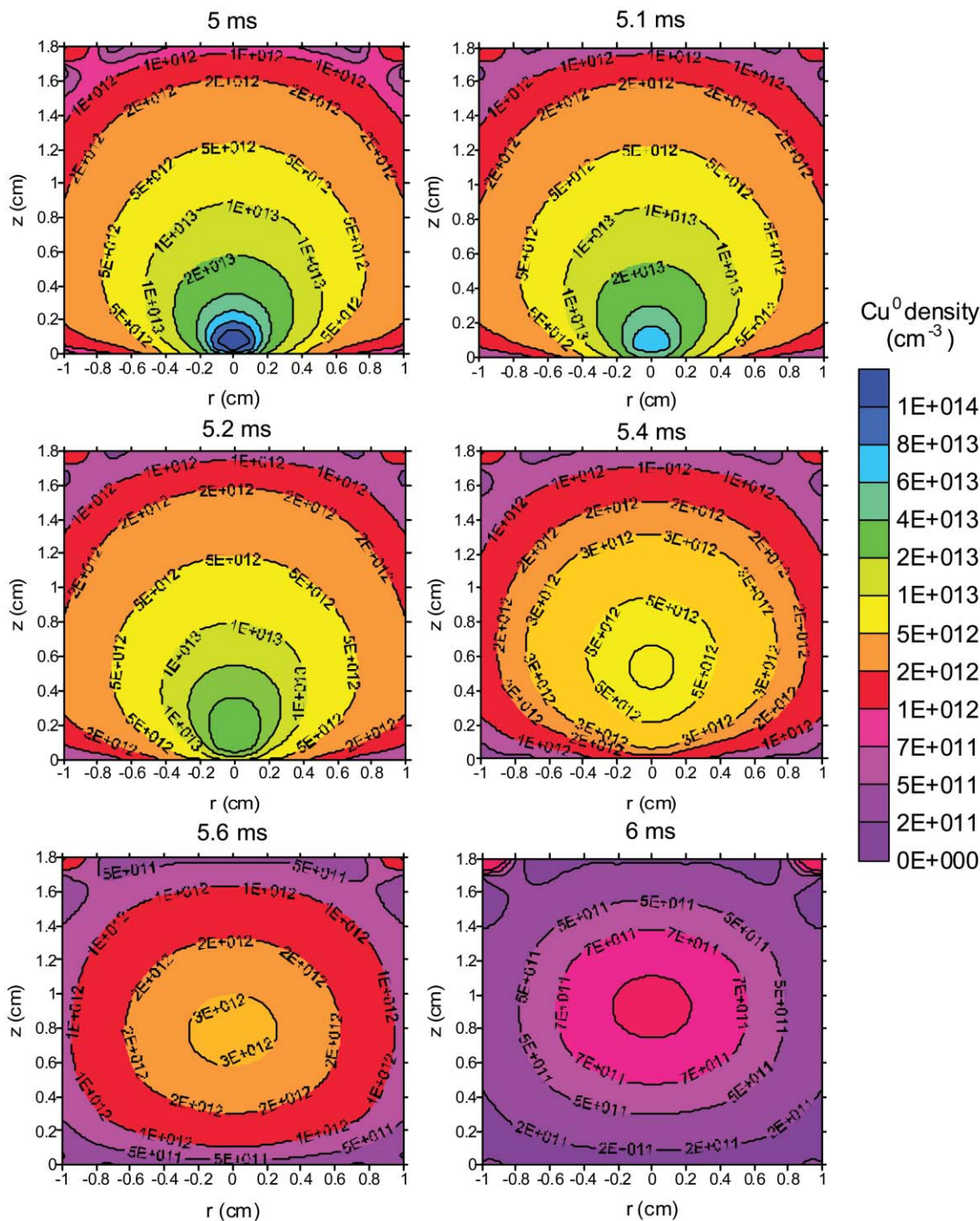


Fig. 8 Calculated two-dimensional density profiles of the sputtered Cu atoms, at different times in the afterglow, for the same conditions as in Fig. 1.

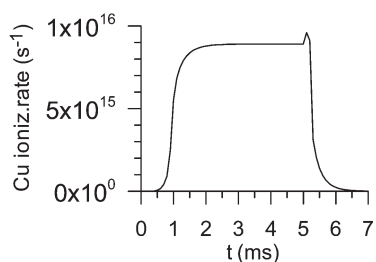


Fig. 9 Calculated ionization rate of the sputtered Cu atoms, integrated over the entire discharge geometry, as a function of time, for the same conditions as in Fig. 1.

3.4.4. Cu^+ ions in the ground state. The calculated two-dimensional Cu^+ ion density profiles, at different times in the afterglow, are illustrated in Fig. 10. The Cu^+ ion density is characterized by a maximum in the middle of the discharge (in the NG), and a low and more or less constant value in the CDS, which is in correlation with the calculated Ar^+ ion density profiles (*cf.* Fig. 3).

At the end of the pulse, the Cu^+ ion density has a maximum of *ca.* $2 \times 10^{10} \text{ cm}^{-3}$. The density was found to increase slightly in the early afterglow, with a maximum value of about $2.7 \times 10^{10} \text{ cm}^{-3}$ at 5.1 ms, and $2.3 \times 10^{10} \text{ cm}^{-3}$ at 5.2 ms, due to Penning ionization (see previously). At later times, the density drops, but the drop is less pronounced than for the Cu atoms. (Note that the Cu^+ ion density is also illustrated at 7 ms in Fig. 10, in contrast to the Cu atom density). The general shape of the Cu^+ ion density profile remains roughly the same, but

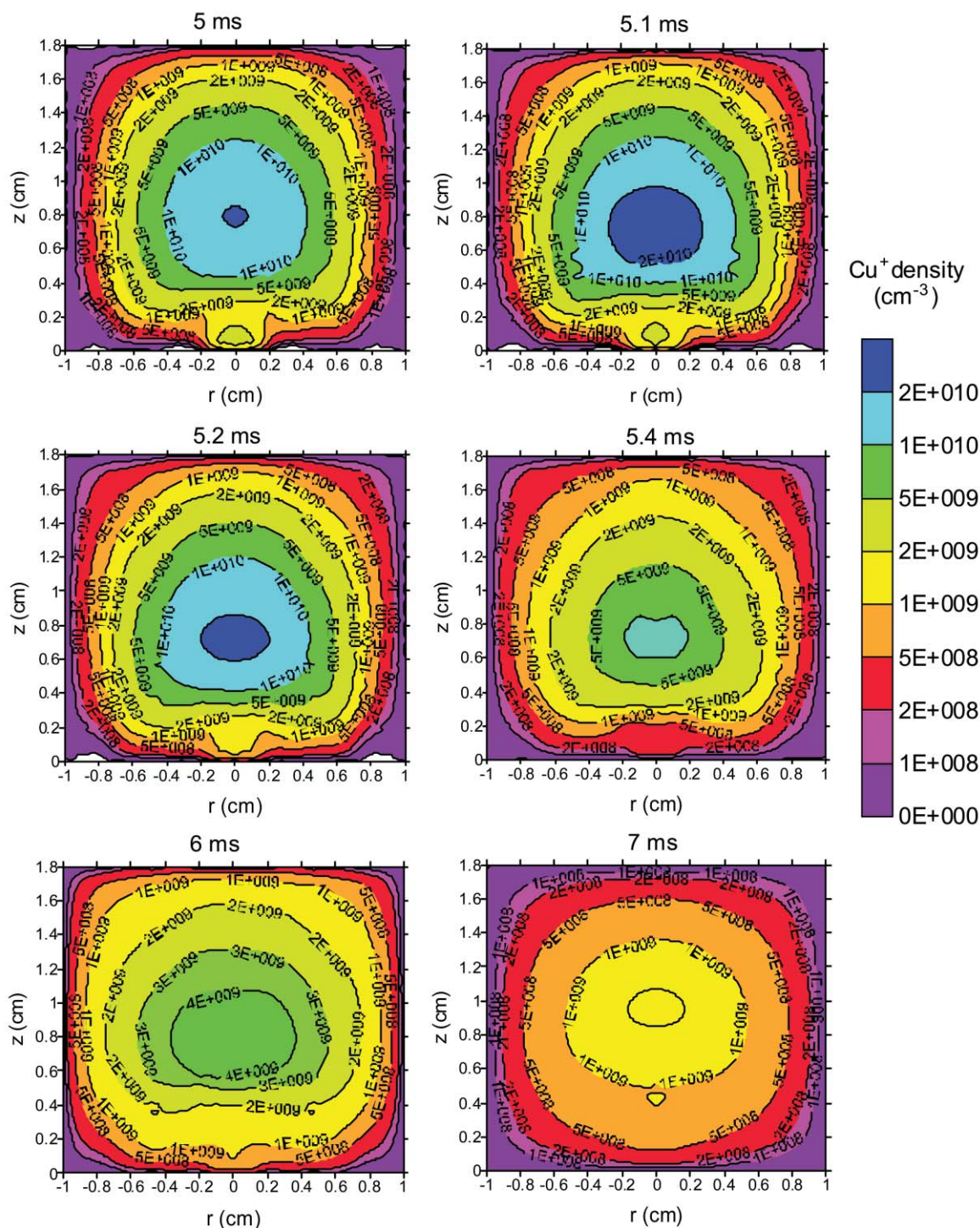


Fig. 10 Calculated two-dimensional density profiles of the Cu^+ ions, at different times in the afterglow, for the same conditions as in Fig. 1.

the specific (nearly constant) shape in the CDS disappears after 5.4 ms, because of the disappearance of the subdivision between CDS and NG (see Fig. 2).

The Cu^+ ions are characterized by a longer lifetime in the afterglow, certainly in comparison with the Ar^+ ions (Fig. 3). This is because the Cu^+ ions continue to be formed by Penning ionization, which is not the case for the Ar^+ ions. This result is in qualitative agreement with observations in the literature. Indeed, the mass spectra of pulsed glow discharges are characterized by a high intensity of Ar^+ ions during the pulse, whereas the Cu^+ ion peaks become dominant in the afterglow (e.g., refs. 1,10–12,25,26).

3.4.5. Cu atoms and Cu^+ ions in the ground state and in excited levels.

The calculated time-behavior of the densities of

the ground state Cu atoms and Cu^+ ions is also illustrated in one dimension (i.e., axial direction, averaged in the radial direction over the region of the cathode diameter) in Fig. 11(a) and (b). These figures also show clearly that the ground state Cu^+ ions show a little increase in density, and have a longer lifetime in the afterglow than the ground state Cu atoms.

More or less the opposite behavior is found for the excited states of the Cu atoms and Cu^+ ions, as appears from Fig. 11(c)–(f). Indeed, Fig. 11(c) illustrates the calculated level populations of the Cu^* atom $3d^{10} 4p \ ^2P_{3/2}$ excited level (at 3.82 eV), at different times during the afterglow. The population density remains nearly constant in the early afterglow, and then drops slowly as a function of time. The reason for this slow drop is the production of this level by radiative decay from higher excited levels, which are produced by ion-electron

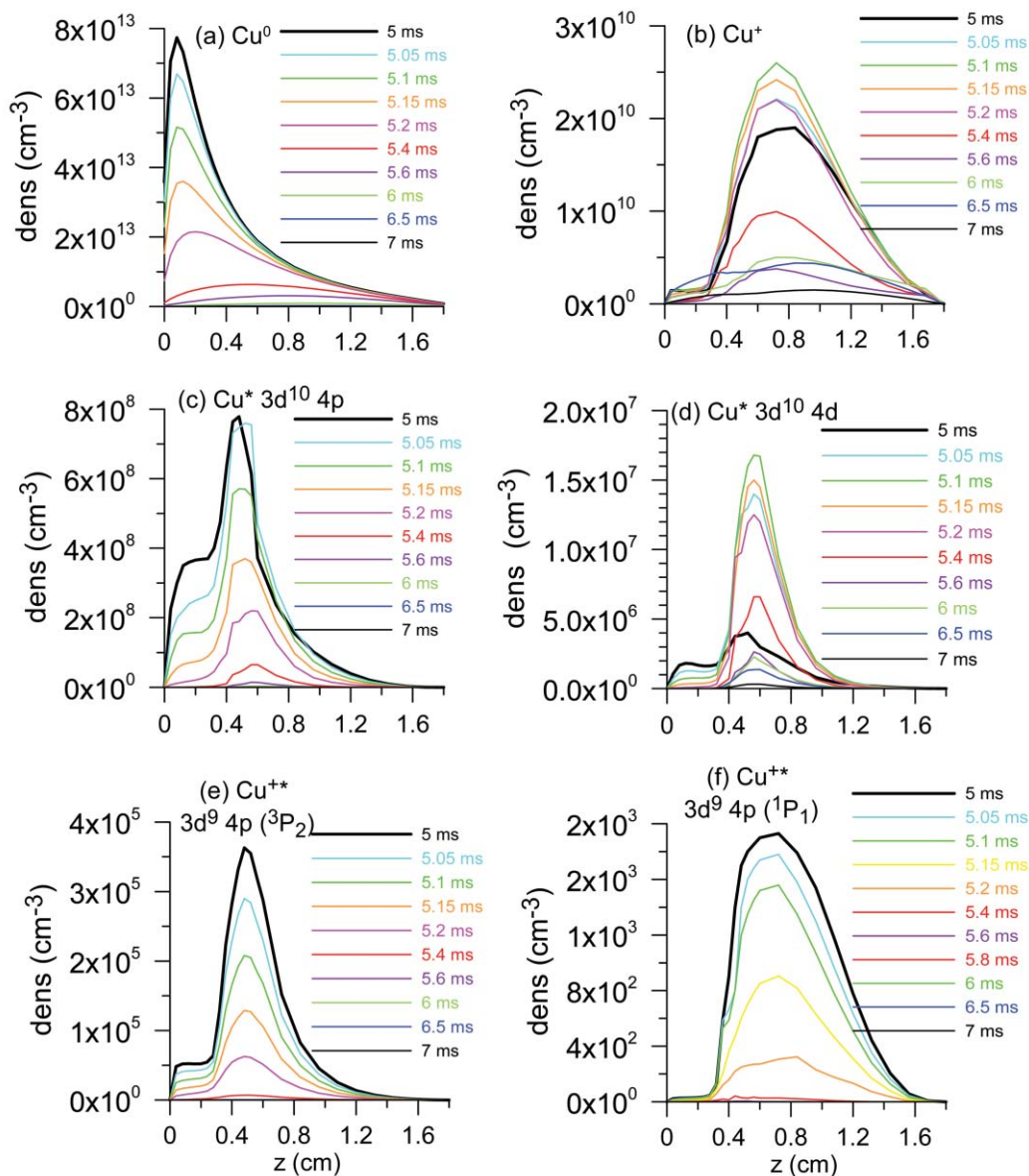


Fig. 11 Calculated one-dimensional density profiles of the Cu atoms (a) and Cu⁺ ions (b) and of several Cu⁰ and Cu⁺ excited levels, at different times in the afterglow, for the same conditions as in Fig. 1. (c) Cu⁰ 3d¹⁰ 4p ²P_{3/2} level (at 3.82 eV), (d) Cu⁰ 3d¹⁰ 4d level (at 6.2 eV), (e) Cu⁺ 3d⁹ 4p (³P₂) level (at 15.96 eV), (f) Cu⁺ 3d⁹ 4p (¹P₁) level (at 16.85 eV).

recombination in the afterglow. Indeed, if the latter process would not occur, the Cu atom excited level population would drop much faster as a function of time. Lifetimes for these states are on the order of 10⁻⁶ s or less. In analogy to the behavior of the Ar* atom excited levels, our model also predicts a rise in population density for the higher excited Cu* atom levels in the early afterglow, and this rise is more pronounced for the highest excited levels. This follows clearly from Fig. 11(d), where the calculated level population of the Cu* atom 3d¹⁰ 4d excited level (*i.e.*, the highest Cu* atom level considered in our collisional-radiative model,⁴³ at *ca.* 6.2 eV) increases considerably as a function of time in the early afterglow. This time-behavior, and the difference between low and high Cu* atom excited levels, are in good correspondence with measurements of Lewis *et al.*²⁸

The calculated Cu⁺ ion excited levels, on the other hand, do not show any rise in densities in the afterglow, as is apparent from Fig. 11(e) and (f). Fig. 11(e) presents the level populations of the Cu⁺ ion 3d⁹ 4p (³P₂) excited level (*i.e.*, the level populated by asymmetric charge transfer with Ar⁺ ions,^{43,57} at 15.96 eV), whereas Fig. 11(f) depicts the level populations of the Cu⁺ 3d⁹ 4p (¹P₁) excited level (at 16.85 eV). The density

profile of the so-called charge transfer level is characterized by a somewhat different shape compared to the other excited Cu⁺* ions, which is explained by the different production mechanism. However, the time-behavior in the afterglow (more specifically, the absence of an afterpeak) was found to be similar for all Cu⁺* ion excited levels (except for the highest level taken into account in the collisional-radiative model). The reason is that electron-Cu²⁺ ion recombination yields the formation of the highest Cu⁺* ion level considered in our model (*i.e.*, the 3d⁹ 5s level, which is an effective level, grouping four different 5s levels; at 21.24 eV),⁴³ but radiative decay from this level to the lower excited Cu⁺* ion levels is found to play a negligible role in the production of the other excited Cu⁺* ion levels.⁴³ Indeed, the latter are predicted to be almost exclusively populated by electron impact excitation from the Cu⁺ ion ground state and lower excited levels, and by asymmetric charge transfer (for the 3d⁹ 4p ³P₂ level).⁴³ The absence of an afterpeak for all Cu⁺* ion excited levels is also in agreement with the experimental observations by Lewis *et al.*²⁸

3.4.6. Optical emission intensities of Cu(I) and Cu(II) lines. In Fig. 12 the optical emission intensities of two Cu(I) lines and

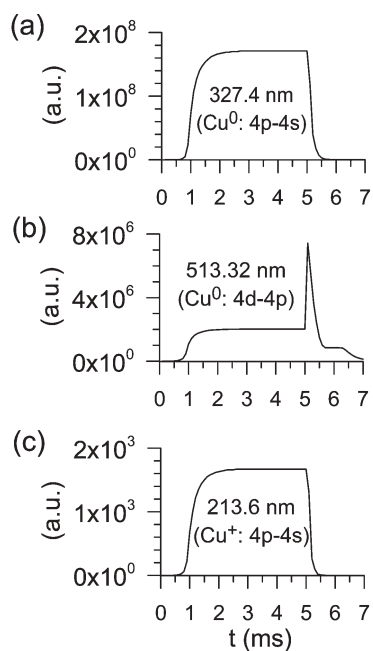


Fig. 12 Calculated optical emission intensities, integrated over the entire discharge length to simulate end-on observation, of some Cu(I) and Cu(II) lines corresponding to different transitions, as a function of time, for the same conditions as in Fig. 1. (a) Cu(I) 327.4 nm (Cu^0 4p-4s transition), (b) Cu(I) 515.32 nm (Cu^0 4d-4p transition), (c) Cu(II) 213.6 nm (Cu^+ 4p-4s transition).

one Cu(II) line are plotted as a function of time during and after the pulse. Note that the optical emission intensities are again calculated by integration over the axial direction, to simulate end-on observation. In analogy to the behavior of the excited level populations (see above), the Cu(I) 327.4 nm line, which originates from a low Cu^* atom excited level (*i.e.*, $3d^{10} 4p^2 P_{1/2}$, at 3.79 eV), does not show any afterpeak (see Fig. 12(a)), whereas the Cu(I) 515.32 nm line, which decays from a high Cu^* atom excited level (*i.e.*, a $3d^{10} 4d$ level, at ~ 6.2 eV), is characterized by a pronounced peak in the early afterglow (Fig. 12(b)). Hence, the afterpeak/plateau ratio increases again for the higher excited Cu^* levels. Finally, all calculated Cu(II) lines were found to behave similarly as a function of time, with the absence of an afterpeak, as is illustrated for the Cu(II) 213.6 nm line in Fig. 12(c). This behavior is in qualitative agreement with the measured data of Lewis *et al.*²⁸

3.5. Possible electron-ion recombination mechanisms in the afterglow

3.5.1. Recombination rates required in the Ar and Cu collisional-radiative models. As mentioned above, the afterpeak in the calculation results for excited level populations and optical emission intensities, is obtained by assuming in the Ar and Cu collisional-radiative models certain values for the electron-ion recombination rate to the highest excited levels in the afterglow. For Ar, a maximum recombination rate of about $6 \times 10^{19} \text{ cm}^{-3} \text{ s}^{-1}$ was required to yield sufficient population of the Ar^* atom excited levels. This is extremely high, certainly if one takes into account that the electron-ion recombination rate at the end of the pulse was calculated to be about 10^8 cm^{-3} , based on the rate constant for electron- Ar^+ ion collisional-radiative recombination at an electron temperature of ~ 1 eV (see below) and the electron and Ar^+ ion densities calculated at the end of the pulse (see Fig. 3).

For Cu, the maximum recombination rate needed in the model to yield sufficient population of the highest excited Cu^* atom levels, amounted *ca.* $3 \times 10^{15} \text{ cm}^{-3} \text{ s}^{-1}$. Note that the

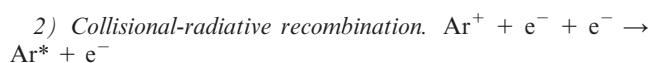
recombination rate needed for sufficient recombination to the Cu^{+*} highest excited levels was not critical, because radiative decay from this highest excited level was found to be negligible as population mechanism for the Cu^{+*} excited levels anyway (see above).

The question arises how electron-ion recombination can become so important in the afterglow, when it is almost negligible during the pulse regime (as well as in dc discharges).^{34,58} As mentioned above, Biondi⁴⁴ has pointed out that the electrons might quickly lose their energy by collisions with gas atoms upon pulse termination, and come to thermal equilibrium with the gas during the first 100 μs of the afterglow, at a gas pressure around 1 Torr. As a result, the rate of loss of electrons by diffusion and subsequent recombination at the cell walls will decrease drastically, and the electrons will be trapped in the bulk of the plasma, so that the electron density is expected to increase upon pulse termination.⁴⁴ Moreover, the electron-ion recombination rate coefficients typically increase with decreasing electron energy (see below). Hence, from the higher electron density, in combination with the higher recombination rate coefficients, the increase in electron-ion recombination in the afterglow is indeed expected.

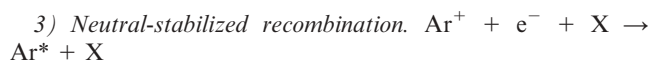
3.5.2. Overview of the different electron-ion recombination mechanisms for Ar. Based on the above requirement for the significant rise in recombination rate we have to investigate which recombination mechanisms might play a role in the afterglow of the pulsed glow discharge under study. From the conservation laws of momentum and energy, it follows that a simple two-body coalescence is not allowed for atomic ions.⁵⁹ Hence, a third body should take part in the reaction (either an electron, atom, molecule or photon), to take away the excess energy. For Ar four recombination mechanisms are in principle possible:



Here, the excess energy is carried away by a photon. The rate coefficient for various kinds of ions is reported to be about 10^{-11} – $10^{-12} \text{ cm}^3 \text{ s}^{-1}$ for thermal electrons ($T_e \sim 300 \text{ K}$).⁶⁰



This mechanism is also called three-body recombination with an electron as third body. The recombination rate coefficient for various ions is a strong function of the electron temperature,⁶¹ as is illustrated in Fig. 13(a): $k_{\text{cr}} = 10^{-19} \left(\frac{T_e}{300}\right)^{-9/2}$ with T_e in K, and k_{cr} in $\text{cm}^6 \text{ s}^{-1}$.



This process is also called three-body recombination with an atom or molecule (X) as third body. An important difference with collisional-radiative recombination is the very small fraction of energy lost when electrons make elastic collisions with atoms or molecules, rather than with electrons. However, in the case of molecules acting as the energy-removing third body, a considerable fraction of the electron energy can be removed as a result of low energy inelastic collisions, leading to excitation of the internal rotation and vibration states of the molecule.^{61,62}

In an Ar glow discharge, however, the most straightforward third body is an Ar atom. Since the energy-removing process by atoms is very inefficient in comparison to molecules, this results generally in small rate coefficients.⁶¹ We did not find any formula for the rate coefficient as a function of electron temperature in the case of Ar, but Massey and Burhop⁶⁰ estimated $k_{\text{nsr}} \sim 10^{-11} \times p$ (where p is expressed in Torr, and k_{nsr} is in $\text{cm}^3 \text{ s}^{-1}$), yielding a rate coefficient of $\sim 10^{-11} \text{ cm}^3 \text{ s}^{-1}$

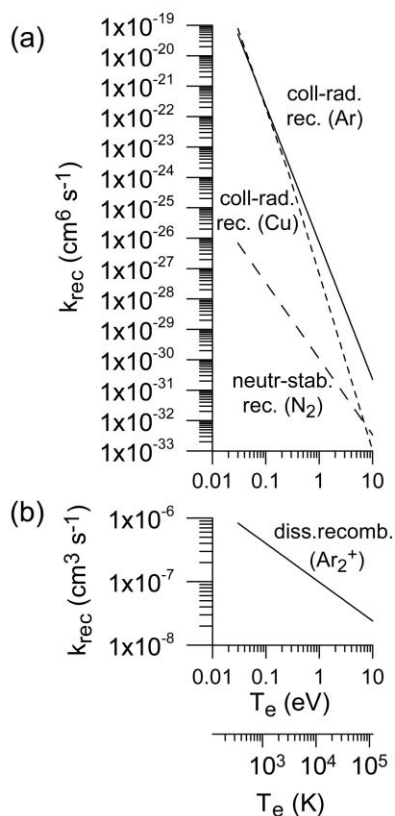


Fig. 13 Recombination rate coefficients for the formation of Ar and Cu atoms, as a function of electron temperature. (a) collisional-radiative recombination of Ar^+ (solid line), of Cu^+ (small dashed line) and neutral-stabilized recombination (with N_2) (wide dashed line); (b) dissociative recombination of Ar_2^+ . For information, the electron temperature (x -axis) is given both in eV and in K.

at 1 Torr, hence comparable to radiative recombination (see above).

For comparison with collisional-radiative recombination, Fig. 13(a) illustrates the recombination rate coefficient as a function of electron temperature for the case of N_2 molecules acting as third body.^{61,62} It is apparent that even for N_2 molecules the neutral-stabilized recombination rate coefficient is many orders of magnitude lower than the collisional-radiative recombination rate coefficient. Hence, even correcting for the generally larger molecule (or atom) density compared to electron density, neutral-stabilized recombination appears to be of minor importance for N_2 as third body. Therefore, this will certainly hold true for an Ar atom as third body.

4) Dissociative recombination. $\text{Ar}_2^+ + e^- \rightarrow \text{Ar}^* + \text{Ar}$

For molecular ions a two-body recombination process is possible because the collision product can dissociate and the recombination energy can be converted into kinetic and potential energy of the dissociation products. It is interesting to mention that, more than 60 years ago, Bates pointed out a discrepancy between theory and experiment on recombination rates in Ar discharge tubes,⁶³ which is in a sense similar to the discrepancy between model and experiment for the analytical pulsed glow discharge discussed in the Introduction. Indeed, the experimentally observed recombination rate coefficient in the Ar discharge was much higher than predicted from theory.⁶³ However, in the theory, dissociative recombination (with Ar_2^+ ions) was precluded, because molecular ions were assumed to be of minor importance in the discharge.⁶³ About ten years later, it was pointed out by Bates^{64,65} and by Biondi and coworkers^{66–69} that dissociative recombination with molecular ions is characterized by a much higher rate coefficient than recombination with atomic ions. Hence, it can be more

important in rare gases, even when the molecular ions are of minor importance than the atomic ions. In more recent work, molecular ions (Ar_2^+ or He_2^+) and dissociative recombination are even expected to play a dominant role during the plasma decay phase of rare gas plasmas at atmospheric pressure (*i.e.*, when molecular ions are formed more easily) (*e.g.*, refs. 70–72). In ref. 73, a transition from collisional-radiative recombination to dissociative recombination was investigated in an Ar afterglow plasma, in the pressure range of 5–18 Torr.

Although molecular ions are formed more easily at high pressure (mainly due to Ar^+ ion collisions with two Ar gas atoms,⁷⁴) they are also present in glow discharges at a typical pressure of 1 Torr, where they are created mainly by associative ionization (either by collisions of two Ar^* metastable atoms, or by the collision of a highly excited Ar^* atom with a ground state Ar atom).⁷⁵ In a dc glow discharge, at similar pressure and voltage as investigated in the present work, the Ar_2^+ ion density was calculated to be about 2.5% of the Ar^+ ion density.⁷⁵

The rate coefficient for dissociative recombination is a much weaker function of electron temperature,^{76,77} as is depicted in Fig. 13(b): $k_{\text{dr}} = 9 \times 10^{-7} \left(\frac{T_e}{300}\right)^{-0.61}$ where the electron temperature (T_e) is given in K, and k_{dr} is in $\text{cm}^3 \text{s}^{-1}$. The absolute value, on the other hand, is considerably higher, so that this process might be important, even if the Ar_2^+ ion density is a few orders of magnitude lower than the Ar^+ ion density (see above).

However, whereas for the above recombination processes with Ar^+ ions, the Ar^* atoms are created in the highest excited levels,^{61,77} this is generally not the case for dissociative recombination.^{61,69} Indeed, the ground state energy of the molecular ion is equal to the ionization energy of Ar (*i.e.*, 15.76 eV), minus the dissociation energy of Ar_2^+ (*i.e.*, 1.05 eV),^{78,79} yielding a value of 14.71 eV. Hence, only Ar^* atom excited levels with energy lower than 14.71 eV can be populated by dissociative recombination of Ar_2^+ ions (at least if the Ar_2^+ ions are in the ground vibrational level and if the electrons have low energy). Indeed, population of the Ar^* ($3p^5$) $4p$, $4p'$, $3d$ and $5d$ levels has been reported for dissociative recombination of Ar_2^+ ions.^{77,80–84} Since Jackson *et al.*³⁰ have found experimentally that the afterpeak emission is highest for the highest excited levels (*i.e.*, the levels lying close to the ionization potential), this seems to rule out electron- Ar_2^+ ion recombination in the afterglow. The latter would be confirmed by the complete absence of Ar_2^+ in the afterpeak.³⁰

Before precluding this mechanism completely, it is, however, interesting to realize that when the Ar_2^+ ions themselves would be populated in high vibrational states, they could in principle give rise to the production of higher excited Ar^* levels. There is some evidence in the literature for dissociative recombination of vibrationally excited molecular ions (He_2^+ , Ne_2^+ , Ar_2^+ , Xe_2^+ , H_2^+), giving rise to atoms in highly excited levels.^{68,85–90} The molecular ions can be formed in high vibrational levels by a collision of an atomic ion with two gas atoms (“atomic ion to molecular ion conversion”),⁸⁵ as well as by associative ionization of highly excited atoms.^{86,91,92} The probability for vibrational relaxation appears to be quite low; hence, the molecular ions can remain vibrationally excited for a long time.^{68,85,89} In the case of H_2^+ , it has been demonstrated that the rate of dissociative recombination of H_2^+ ions in high vibrational levels ($v \geq 5$) exceeds the rate for the lower vibrational levels by two orders of magnitude.^{87–89} The latter observation can, however, not be generalized to other molecular ions.⁶¹ Indeed, the dependence of the dissociative recombination rate on the vibrational excitation of the molecular ion depends on the overlap between the initial (molecular ion) state and the intermediate (excited molecule) state. Hence, the detailed curve crossings for a particular molecular system determine the dependence on vibrational state.⁶¹ For Ar_2^+ ions, it has even been suggested that the rate

coefficient for dissociative recombination from the ground state is higher than for the vibrationally excited levels.⁹⁰

As mentioned above, we have calculated in a previous work⁷⁵ the density of Ar_2^+ ions in a dc glow discharge, at similar operating conditions as used here during the pulse, and we have also investigated the production and loss mechanisms. Associative ionization, both by collisions of two Ar^* metastable atoms ($\text{Ar}_m^* + \text{Ar}_m^* \rightarrow \text{Ar}_2^+ + e^-$), and by collisions of highly excited Ar^* atoms (with energy above 14.7 eV) with Ar ground state atoms ($\text{Ar}^* + \text{Ar} \rightarrow \text{Ar}_2^+ + e^-$), appeared to be the dominant production mechanisms (with relative contributions of about 40 and 60%, respectively), whereas conversion from atomic to molecular ions ($\text{Ar}^+ + \text{Ar} + \text{Ar} \rightarrow \text{Ar}_2^+ + \text{Ar}$) accounted for only 1%, at a typical pressure around 1 Torr.⁷⁵ Applying this information to the afterglow of the pulsed glow discharge, where the highly excited Ar^* atomic levels are strongly populated (see above), the Ar_2^+ ions might be efficiently created in high vibrational levels by associative ionization. This is of course only a speculation, not based on quantitative data or modeling predictions. Modeling these processes is not possible at this stage because of too little fundamental understanding of these phenomena, but we should keep it in mind as a possible mechanism to account for the afterglow behavior.

Finally, note that dissociative recombination, leading to excited Ar^* atoms, can in principle also occur with other molecular ions present in the Ar glow discharge, such as ArH^+ , and the rate coefficient for dissociative recombination of ArH^+ is in the same order as for the Ar_2^+ ions.⁹³ Jackson *et al.* measured a brief increase in the ArH^+ intensity in the first $\sim 50 \mu\text{s}$ of the afterpeak, followed by a very fast decay, suggesting that electron-ion recombination is indeed the dominant destruction channel.³⁰ However, the energy of ArH^+ ions in the ground state (*i.e.*, 9.8 eV, equal to the ionization potential of H: 13.6 eV, minus the dissociation energy of ArH^+ : 3.8 eV) is even less favorable for producing Ar^* atoms in highly excited levels. Hence, we will not go deeper into this last possibility.

3.5.3. Electron-ion recombination mechanisms for Cu. In principle, the same recombination mechanisms as outlined above, can occur also for Cu. However, based on the above discussion for Ar, we will rule out the mechanisms of radiative recombination and neutral-stabilized recombination. Dissociative recombination (with Cu_2^+ or CuAr^+) might in principle take place, but the same arguments would have to be applied as to dissociative recombination of Ar_2^+ ions (*i.e.*, high population density in high vibrational levels is required). Because we found no data in the literature, it makes no sense to go into deeper detail on this process. Hence, we will concentrate here only on collisional-radiative recombination: $\text{Cu}^+ + e^- + e^- \rightarrow \text{Cu}^* + e^-$.

The rate coefficient for this process is also a strong function of the electron energy (see Fig. 13(a)), and can be expressed as:⁴³

$$k_{\text{crr}} = 1.154 \times 10^{-6} \rho T_e^{-5} \text{ cm}^6 \text{ s}^{-1} \text{ (for } T_e < 3100 \text{ K)}$$

$$k_{\text{crr}} = 7.16 \times 10^{-4} \rho T_e^{-5.8} \text{ cm}^6 \text{ s}^{-1} \text{ (for } T_e > 3100 \text{ K)}$$

where ρ is the Coulomb logarithm: $\rho = Z^3 \left[\sqrt{Z^2 + 1} \right]$ with Z being the charge state of the ion.

3.5.4. Estimation on the required rise in electron density, and the electron-ion recombination mechanism accounting for the observed afterpeak. Based on the assumption that the electron temperature thermalizes to ~ 0.05 eV in the early afterglow (*i.e.*, in *ca.* 100 μs , following Biondi,⁴⁴) and on the above recombination rate coefficients, we can now make some

estimates on the rise in electron density needed to account for the electron-ion recombination rates in the collisional-radiative models (*i.e.*, $\sim 6 \times 10^{19} \text{ cm}^{-3} \text{ s}^{-1}$ for Ar, and $\sim 3 \times 10^{15} \text{ cm}^{-3} \text{ s}^{-1}$ for Cu, see above).

Note that we don't know how the Ar^+ and Ar_2^+ ion densities will behave upon pulse termination. Possibly, the Ar^+ ion density will also increase to the same extent as the electron density, due to the process of ambipolar diffusion (*i.e.*, the simultaneous diffusion of electrons and ions, as a result of their space charge field), leading to a similar drop in loss rate for Ar^+ ions as for electrons. On the other hand, a rise in Ar^+ ion intensity is experimentally not observed in the afterglow.²⁸⁻³⁰ Therefore, we will give estimates for the rise in electron density in a certain range, corresponding (i) to the assumption of a similar rise in Ar^+ ion density as for the electron density, and (ii) the assumption of an Ar^+ ion density equal to the value calculated at the end of the pulse (*i.e.*, $8 \times 10^{10} \text{ cm}^{-3}$; see Fig. 3).

The Ar_2^+ ion density has not been computed in the present model. However, as mentioned above, the Ar_2^+ density was calculated to be about 2.5% of the Ar^+ ion density for a dc glow discharge, at similar pressure and voltage as investigated here.⁷⁴ This would suggest an Ar_2^+ density at the end of the pulse equal to $2 \times 10^8 \text{ cm}^{-3}$. On the other hand, as discussed above, the Ar_2^+ ion density might also increase considerably because of associative ionization of highly excited Ar^* atomic levels, but it is impossible to predict how much this rise would be.

In the following, the required rise in electron density will be calculated for the four recombination mechanisms of Ar, as well as for Cu.

1) *Ar: Radiative recombination.* $\text{Rate}_{\text{rr}} = k_{\text{rr}} n_e n_{\text{Ar}^+}$, and $k_{\text{rr}} \sim 10^{-11} - 10^{-12} \text{ cm}^3 \text{ s}^{-1}$: Hence, the product of electron and Ar^+ ion density should be $\sim 6 \times 10^{30} - 6 \times 10^{31} \text{ cm}^6$, yielding an electron density in the range $\sim 3 \times 10^{15} - 8 \times 10^{20} \text{ cm}^{-3}$ (depending on the assumption on Ar^+ ion density, see above).

2) *Ar: Collisional-radiative recombination.* $\text{Rate}_{\text{crr}} = k_{\text{crr}} (n_e)^2 n_{\text{Ar}^+}$, and $k_{\text{crr}} \sim 5.2 \times 10^{-21} \text{ cm}^6 \text{ s}^{-1}$ (at $T_e = 0.05$ eV; see Fig. 13): Hence, the product $(n_e)^2 n_{\text{Ar}^+}$ should be $\sim 10^{40} \text{ cm}^9$, giving rise to an electron density in the range $\sim 2 \times 10^{13} - 4 \times 10^{14} \text{ cm}^{-3}$ (depending again on the assumption for the Ar^+ ion density).

3) *Ar: Neutral-stabilized recombination.* $\text{Rate}_{\text{nsr}} = k_{\text{nsr}} n_e n_{\text{Ar}^+}$, and $k_{\text{nsr}} \sim 10^{-11} \text{ cm}^3 \text{ s}^{-1}$ at 1 Torr: Therefore, the product of electron and Ar^+ ion densities should be $\sim 6 \times 10^{30} \text{ cm}^6$, corresponding to an electron density of $3 - 8 \times 10^{15} \text{ cm}^{-3}$.

4) *Ar: Dissociative recombination.* $\text{Rate}_{\text{dr}} = k_{\text{dr}} n_e n_{\text{Ar}_2^+}$, and $k_{\text{dr}} \sim 6 \times 10^{-7} \text{ cm}^3 \text{ s}^{-1}$ at 0.05 eV (see Fig. 12(b)): Assuming that the Ar_2^+ ion density is about $2 \times 10^9 \text{ cm}^{-3}$, the product of electron and Ar_2^+ ion densities should be $\sim 10^{26} \text{ cm}^6$, yielding an electron density of $5 \times 10^{16} \text{ cm}^{-3}$. On the other hand, if we assume that the Ar_2^+ ion density rises by several orders of magnitude as a result of associative ionization (see above), the rise in electron density can be more moderate.

5) *Cu: Collisional-radiative recombination.* $\text{Rate}_{\text{crr}} = k_{\text{crr}} (n_e)^2 n_{\text{Cu}^+}$, and $k_{\text{crr}} \sim 6 \times 10^{-21} \text{ cm}^6 \text{ s}^{-1}$ at 0.05 eV (see Fig. 12(a)). Assuming for the Cu^+ ion density a value of $2 \times 10^{10} \text{ cm}^{-3}$ (see Fig. 10), yields for the electron density a value of $\sim 5 \times 10^{12} \text{ cm}^{-3}$.

These estimations all suggest that the electron density should increase considerably in the afterglow. The most plausible mechanism for Ar, based on the estimated rise in electron densities, would be collisional-radiative recombination. If the Ar^+ ion density would increase to the same extent as the electron density, a value of $2 \times 10^{13} \text{ cm}^{-3}$ in the early afterglow

would be predicted. This is an increase of more than a factor 100 compared to the value at the end of the pulse. Although this is a dramatic increase, we think it is not too unrealistic keeping in mind the considerable uncertainties in this predicted value.

For Cu, the rise in electron density, also based on collisional-radiative recombination, was calculated to be $5 \times 10^{12} \text{ cm}^{-3}$. This is somewhat lower than our predicted value for Ar. However, this difference is probably not significant. It is attributed to the different number of excited levels taken into account in the Ar and the Cu collisional-radiative models.^{38,43} Indeed, for Ar 64 excited levels were included in our model, and electron-ion recombination is only assumed to populate the two highest levels (*i.e.*, belonging to the primed and unprimed system, respectively, with different ionization limits; see ref. 38), which then subsequently populate the lower excited levels by radiative decay. Hence, many radiative steps (with accompanying loss in population rates) will be necessary to populate, for instance, the 7s and 7d levels, investigated in this work to compare with the experiments. For Cu, on the other hand, only eight atomic levels were considered in our model, of which the $3d^{10} 4d$ level (investigated in this work, see above) is the highest one. Hence, this level is directly populated by electron-ion recombination, which explains why a lower recombination rate gives a sufficiently high afterpeak.

This difference illustrates once more that the predictions made above for the electron density rise are only qualitative. However, it is the best we can do at this moment, because there are still too many uncertainties to carry out a numerical simulation. We hope that this investigation can be useful for further experimental studies on pulsed glow discharges. An interesting experiment, to check our predictions, would be to measure the electron temperature and density in the early afterglow, *e.g.*, by Langmuir probes or Thomson scattering.

If no appreciable rise in electron density would be observed in the afterglow, then collisional-radiative recombination becomes less probable. The only other possibility would then be dissociative recombination with Ar_2^+ ions, if the latter would be efficiently populated in high vibrational levels by associative ionization of the highly excited Ar^* atoms. However, the latter speculation is not based on quantitative data or model predictions. Moreover, King and coworkers^{28–30} observed a similar behavior for the Ar^* and Cu^* excited levels, which is in favor of collisional-radiative recombination as the mechanism accounting for the afterglow, unless a similar dissociative recombination mechanism for Cu would come into play (such as from CuAr^+ , Cu_2^+ or CuH^+). In any case, before dissociative recombination could ever become accepted as an important mechanism for populating the highly excited levels, some more dedicated experiments would have to be conducted in this direction. This would include the study of the behavior of the molecular ions in ground and vibrational levels, and of the highest excited atomic levels.

Finally, another interesting aspect of recombination to consider, both experimentally and theoretically, is the recombination of excited ion species with electrons and a third body. Lewis *et al.* have observed significant tailing in the afterpeak emissions of the doubly excited states of copper atoms.²⁸ See, for example, the emissions from the $4s4p$ band to the $4s^2$ band, represented by the line at 333.79 nm, in Fig. 3 of ref. 28. Because the lifetimes of the excited states cannot alone account for the delayed emissions of these lines, there must be another reason for the delay in observed emissions from these levels. Furthermore, emissions from doubly excited states of copper atoms above the IP of the singly excited system were also observed to have significant tailing in the afterpeak.⁹⁴ It would be interesting to determine whether the metastable copper ion states at ~ 2.72 eV have a significantly lower probability of recombining than ground state copper ions. In general, it would be interesting to learn more about highly excited

Rydberg states in pulsed glow discharges. They behave in a semi-metastable way, and therefore, they might also play a significant role in the mechanism of collisional-radiative cascade. However, not much appears to be known yet about highly excited Rydberg states in analytical glow discharges, *e.g.*, how numerous are they. Mason *et al.* have suggested that they play an important role in fast flow glow discharges, in stepwise ionization, as precursors for most ions observed in GDMS.⁹⁵ Clearly, there is still much fundamental knowledge to be learned about highly excited states and recombination processes in pulsed glow discharges.

4. Conclusion

We have applied our modeling network, developed earlier for an Ar glow discharge with Cu cathode, to a millisecond pulsed glow discharge, in order to investigate the afterglow mechanisms. It is expected that the electron energy drops considerably upon pulse termination, leading to a significant rise in electron density. The latter, in combination with a rise in recombination rate coefficients at lower electron energy, appears to be responsible for the efficient recombination in the afterglow, giving rise to the experimentally observed afterpeaks. Because this cannot yet be simulated with our model, we have worked in reversed order. We have calculated how large the recombination rates (both for Ar and Cu) have to be, to account for the experimentally observed afterpeaks, and based on this calculation, we have investigated which electron-ion recombination mechanisms might play a role, and what should be the corresponding rise in electron density.

This lead us to conclude that collisional-radiative recombination (*i.e.*, three-body recombination with an electron as third body) is the most plausible candidate to account for the afterpeaks, both for Ar and Cu, but it requires a rise in electron density in the early afterglow of about two orders of magnitude in comparison to the value at the end of the pulse.

It would be very interesting if this electron density (as well as the electron temperature) could be measured in the early afterglow of the ms-pulsed glow discharge, to check our investigations. If experimental data would elucidate that this rise in electron density is unrealistically high, a possible alternative would be dissociative recombination with molecular ions (such as Ar_2^+) in high vibrational levels. Although this possibility is currently based on several speculations, we think that it cannot yet completely be ruled out. This alternative would almost certainly be more significant in higher pressure discharges where the formation rates of Argon dimers is considerably faster. We hope that our investigation can motivate more experiments in this field, such as the measurement of electron density and temperature, and the investigation of the time-behavior of various ions (Ar^+ , Ar_2^+) in the afterglow, and of highly excited levels of molecular ions and atoms.

Acknowledgements

A. Bogaerts is indebted to the Flemish Fund for Scientific Research for financial support. The authors also acknowledge financial support from the IUAP-V project. Finally, we would like to thank F. King, J. van der Mullen, A. Phelps and J. Glosik for the many interesting discussions.

References

- 1 W. W. Harrison, W. Hang, X. Yan, K. Ingeneri and C. Shilling, *J. Anal. At. Spectrom.*, 1997, **12**, 891.
- 2 W. W. Harrison, *J. Anal. At. Spectrom.*, 1998, **13**, 1051.
- 3 W. W. Harrison, C. Yang and E. Oxley, *Anal. Chem.*, 2001, **73**, 480A.

- 4 W. O. Walden, W. Hang, B. W. Smith, J. D. Winefordner and W. W. Harrison, *Fresenius' J. Anal. Chem.*, 1996, **355**, 442.
- 5 X. Yan, W. Hang, B. W. Smith, J. D. Winefordner and W. W. Harrison, *J. Anal. At. Spectrom.*, 1998, **13**, 1033.
- 6 C. Yang and W. W. Harrison, *Spectrochim. Acta, Part B*, 2001, **56**, 1195.
- 7 X. Yan, K. Ingeneri, W. Hang and W. W. Harrison, *J. Anal. At. Spectrom.*, 2001, **16**, 819.
- 8 W. Hang, C. Baker, B. W. Smith, J. D. Winefordner and W. W. Harrison, *J. Anal. At. Spectrom.*, 1997, **12**, 143.
- 9 R. E. Steiner, C. L. Lewis and F. L. King, *Anal. Chem.*, 1997, **69**, 1715.
- 10 D. C. Duckworth, D. H. Smith and S. A. McLuckey, *J. Anal. At. Spectrom.*, 1997, **12**, 43.
- 11 C. L. Lewis, E. S. Oxley, C. K. Pan, R. E. Steiner and F. L. King, *Anal. Chem.*, 1999, **71**, 230.
- 12 C. Yang, M. Mohill and W. W. Harrison, *J. Anal. At. Spectrom.*, 2000, **15**, 1255.
- 13 A. Bengtson, C. Yang and W. W. Harrison, *J. Anal. At. Spectrom.*, 2000, **15**, 1279.
- 14 Y. Su, Z. Zhou, P. Yang, X. Wang and B. Huang, *Spectrochim. Acta, Part B*, 1997, **52**, 633.
- 15 C. Yang, K. Ingeneri and W. W. Harrison, *J. Anal. At. Spectrom.*, 1999, **14**, 693.
- 16 E. Oxley, C. Yang and W. W. Harrison, *J. Anal. At. Spectrom.*, 2000, **15**, 1241.
- 17 C. Yang, K. Ingeneri, M. Mohill and W. W. Harrison, *J. Anal. At. Spectrom.*, 2000, **15**, 73.
- 18 R. E. Steiner, C. L. Lewis and V. Majidi, *J. Anal. At. Spectrom.*, 1999, **14**, 1537.
- 19 V. Majidi, M. Moser, C. Lewis, W. Hang and F. L. King, *J. Anal. At. Spectrom.*, 2000, **15**, 19.
- 20 C. L. Chakrabarti, K. L. Headrick, J. C. Hutton, Z. Bicheng, P. C. Bertels and M. H. Back, *Anal. Chem.*, 1990, **62**, 574.
- 21 C. Pan and F. L. King, *J. Am. Soc. Mass Spectrom.*, 1993, **4**, 727.
- 22 C. Pan and F. L. King, *Anal. Chem.*, 1993, **65**, 3187.
- 23 W. Hang, W. O. Walden and W. W. Harrison, *Anal. Chem.*, 1996, **68**, 1148.
- 24 W. W. Harrison and W. Hang, *J. Anal. At. Spectrom.*, 1996, **11**, 835.
- 25 F. L. King and C. Pan, *Anal. Chem.*, 1993, **65**, 735.
- 26 J. A. Klingler, C. M. Barshick and W. W. Harrison, *Anal. Chem.*, 1991, **63**, 2571.
- 27 J. A. Klingler, P. J. Savickas and W. W. Harrison, *J. Am. Soc. Mass Spectrom.*, 1990, **1**, 138.
- 28 C. L. Lewis, G. P. Jackson, S. K. Doorn, V. Majidi and F. L. King, *Spectrochim. Acta, Part B*, 2001, **56**, 487.
- 29 G. P. Jackson, C. L. Lewis, S. K. Doorn, V. Majidi and F. L. King, *Spectrochim. Acta, Part B*, 2001, **56**, 2449.
- 30 G. P. Jackson, PhD Thesis, West Virginia University, 2002.
- 31 A. Bogaerts and R. Gijbels, *J. Anal. At. Spectrom.*, 1998, **13**, 945.
- 32 A. Bogaerts and R. Gijbels, *J. Anal. At. Spectrom.*, 2000, **15**, 1191.
- 33 A. Bogaerts, R. Gijbels and W. Goedheer, *J. Anal. At. Spectrom.*, 2001, **16**, 750.
- 34 A. Bogaerts and R. Gijbels, *J. Anal. At. Spectrom.*, 2000, **15**, 895.
- 35 A. Bogaerts and R. Gijbels, *J. Anal. At. Spectrom.*, 2001, **16**, 239.
- 36 W. W. Harrison, Private communication.
- 37 A. Bogaerts, M. van Straaten and R. Gijbels, *Spectrochim. Acta, Part B*, 1995, **50**, 179.
- 38 A. Bogaerts, R. Gijbels and W. J. Goedheer, *J. Appl. Phys.*, 1995, **78**, 2233.
- 39 A. Bogaerts and R. Gijbels, *J. Appl. Phys.*, 1995, **78**, 6427.
- 40 A. Bogaerts, R. Gijbels and J. Vlcek, *J. Appl. Phys.*, 1998, **84**, 121.
- 41 N. Matsunami, Y. Yamamura, Y. Itikawa, N. Itoh, Y. Kazumata, S. Miyagawa, K. Morita, R. Shimizu and H. Tawara, *At. Data Nucl. Data Tables*, 1984, **31**, 1.
- 42 A. Bogaerts, M. van Straaten and R. Gijbels, *J. Appl. Phys.*, 1995, **77**, 1868.
- 43 A. Bogaerts, R. Gijbels and R. J. Carman, *Spectrochim. Acta, Part B*, 1998, **53**, 1679.
- 44 M. A. Biondi, *Phys. Rev.*, 1952, **88**, 660.
- 45 A. Bogaerts, M. Yan, R. Gijbels and W. Goedheer, *J. Appl. Phys.*, 1999, **86**, 2990.
- 46 C. K. Birdsall and A. B. Langdon, *Plasma Physics via Computer Simulation*, IOP Publishing Ltd., Adam Hilger Series, Bristol, 1991.
- 47 V. Vahedi, G. DiPeso, C. J. Birdsall, M. A. Lieberman and T. D. Rohnlien, *Plasma Sources Sci. Technol.*, 1993, **2**, 261.
- 48 C. Kenty, *Phys. Rev.*, 1928, **32**, 624.
- 49 K. Kano and H. Akatsuka, *Jpn. J. Appl. Phys.*, 2001, **40**, 4701.
- 50 T. Fujimoto, *J. Phys. Soc. Japan*, 1980, **49**, 1569.
- 51 T. Fujimoto, *J. Phys. Soc. Japan*, 1980, **49**, 1561.
- 52 J. A. M. van der Mullen, *Phys. Rep.*, 1990, **191**, 109.
- 53 A. Bogaerts and R. Gijbels, *Phys. Rev. A*, 1995, **52**, 3743.
- 54 A. V. Phelps and J. P. Molnar, *Phys. Rev.*, 1953, **89**, 1202.
- 55 K. Rozsa, A. Gallagher and Z. Donko, *Phys. Rev. E*, 1995, **52**, 913.
- 56 A. Bogaerts, Z. Donko, K. Kutasi, G. Bano, N. Pinhao and M. Pinheiro, *Spectrochim. Acta, Part B*, 2000, **55**, 1465.
- 57 E. B. M. Steers and R. J. Fielding, *J. Anal. At. Spectrom.*, 1987, **2**, 239.
- 58 A. Bogaerts and R. Gijbels, *Spectrochim. Acta, Part B*, 1998, **53**, 1.
- 59 B. Chapman, *Glow Discharge Processes*, Wiley, New York, 1980.
- 60 H. S. W. Massey and E. H. S. Burhop, *Electronic and Ionic Impact Phenomena*, Oxford University Press, New York, 1952.
- 61 M. A. Biondi, in *Applied Atomic Collision Physics, Vol. 3: Gas Lasers*, ed. E. W. McDaniel and W. L. Nighan, Academic Press, New York, 1982, ch. 6.
- 62 D. R. Bates, *J. Phys. B*, 1980, **13**, 2587.
- 63 D. R. Bates, R. A. Buckingham, H. S. W. Massey and J. J. Unwin, *Proc. Royal Soc.*, 1931, **A176**, 322.
- 64 D. R. Bates, *Phys. Rev.*, 1950, **77**, 718.
- 65 D. R. Bates, *Phys. Rev.*, 1950, **78**, 492.
- 66 M. A. Biondi and S. C. Brown, *Phys. Rev.*, 1949, **76**, 1697.
- 67 M. A. Biondi, *Phys. Rev.*, 1951, **83**, 1078.
- 68 M. A. Biondi and T. Holstein, *Phys. Rev.*, 1951, **82**, 962.
- 69 M. A. Biondi, *Phys. Rev.*, 1963, **129**, 1181.
- 70 M. J. van de Sande, P. van Eck, A. Sola, A. Gamero and J. J. A. M. van der Mullen, *Spectrochim. Acta, Part B*, in press.
- 71 M. van de Sande, PhD Dissertation, Eindhoven University of Technology, 2002.
- 72 J. Jonkers, M. J. van de Sande, A. Sola, A. Gamero, A. Rodero and J. J. A. M. van der Mullen, *Plasma Sources Sci. Technol.*, in press.
- 73 A. Funahashi, T. Makihira and S. Takeda, *J. Phys. Soc. Japan*, 1970, **29**, 441.
- 74 R. Johnsen, A. Chen and M. A. Biondi, *J. Chem. Phys.*, 1980, **73**, 1717.
- 75 A. Bogaerts and R. Gijbels, *J. Appl. Phys.*, 1999, **86**, 4124.
- 76 F. J. Mehr and M. A. Biondi, *Phys. Rev.*, 1968, **176**, 322.
- 77 Y.-J. Shiu and M. A. Biondi, *Phys. Rev. A*, 1978, **17**, 868.
- 78 F. L. Mohler, *Phys. Rev.*, 1928, **31**, 187.
- 79 R. E. Huffman and D. Katayama, *J. Chem. Phys.*, 1966, **45**, 138.
- 80 P. Kebarle, R. M. Haynes and S. K. Scarles, *J. Chem. Phys.*, 1967, **47**, 1684.
- 81 M. Guna, L. Simons, K. Hardy and J. Peterson, *Phys. Rev. A*, 1999, **60**, 306.
- 82 T. Okada and M. Sugawara, *Jpn. J. Appl. Phys.*, 1995, **34**, 5829.
- 83 G. E. Veatch and H. J. Oskam, *Phys. Rev. A*, 1970, **1**, 1498.
- 84 L. Frommhold and M. A. Biondi, *Phys. Rev.*, 1969, **185**, 244.
- 85 W. A. Rogers and M. A. Biondi, *Phys. Rev.*, 1964, **134**, A1215.
- 86 X. K. Hu, J. B. A. Mitchell and R. H. Lipson, *Phys. Rev. A*, 2000, **62**, 52712.
- 87 W. J. van der Zande, J. Semaniak, V. Zengin, G. Sundström, S. Rosén, C. Strömholm, S. Datz, H. Danared and M. Larsson, *Phys. Rev. A*, 1996, **54**, 5010.
- 88 M. A. Chibisov, J. B. A. Mitchell, P. J. T. van der Donk, F. B. Yousif and T. J. Morgan, *Phys. Rev. A*, 1997, **56**, 443.
- 89 J. B. A. Mitchell, F. B. Yousif, P. J. T. van der Donk, T. J. Morgan and M. I. Chibisov, *Int. J. Mass Spectrom. Ion Processes*, 1995, **149**(150), 153.
- 90 A. J. Cunningham and R. M. Hobson, *Phys. Rev.*, 1969, **185**, 98.
- 91 R. S. Mulliken, *Phys. Rev.*, 1964, **136**, A962.
- 92 J. Stevefelt, *Phys. Rev. A*, 1973, **8**, 2507.
- 93 R. F. G. Meulenbroeks, A. J. van Beek, A. J. G. van Helvoort, M. C. M. van de Sanden and D. C. Schram, *Phys. Rev. E*, 1994, **49**, 4397.
- 94 G. P. Jackson, C. Lewis and F. L. King, unpublished results.
- 95 R. S. Mason, P. D. Miller and I. P. Mortimer, *Phys. Rev. E*, 1997, **55**, 7462.